DELFT UNIVERSITY OF TECHNOLOGY

DEPARTMENT OF AEROSPACE ENGINEERING

Report LR - 233

EXPERIMENTAL INVESTIGATION OF THE SUPERSONIC FLOW FIELD ABOUT A SLENDER CONE AT HIGH INCIDENCES

by

C. Nebbeling
W.J. Bannink

DELFT - THE NETHERLANDS

November 1976

DELFT UNIVERSITY OF TECHNOLOGY

DEPARTMENT OF AEROSPACE ENGINEERING

Report LR - 233

EXPERIMENTAL INVESTIGATION OF THE SUPERSONIC FLOW FIELD ABOUT A SLENDER CONE AT HIGH INCIDENCES

by

C. Nebbeling

W.J. Bannink

DELFT - THE NETHERLANDS

November 1976

SUMMARY.

The supersonic flow field about a circular cone having a semi-apex angle θ_c = 7.5 deg. has been investigated experimentally at high incidences ($\alpha \approx \theta_c$ to $3\theta_c$). The experiments, carried out at a free stream Mach number of 2.94 are made using a five hole conical probe allowing the determination of the velocity distribution (direction and magnitude) in the complete flow field, including embedded shock waves and the vortex formation at the lee-side. Emphasis is given on the conical character of the inviscid flow regime, in that the quantities like conical Mach number and the direction of the conical streamlines are indicated. The appearance of the detached vortical singularity in the lee-side symmetry plane is detected and also a "near wake" singularity, the latter is due to the two main vortices at both sides of the symmetry plane.

At incidences of about 17 deg. and higher, an embedded region of conical supersonic flow is observed the boundaries of which are formed by the cone surface, the conical-sonic line and a terminating shock wave. At $\alpha \approx 22$ deg. a second embedded shock wave is measured parallel and close to the leeward cone surface and extending slightly across the symmetry plane. This shock wave is generated by the symmetrical vortices having supersonic cross flow velocity components towards the cone surface at both sides of the symmetry plane.

The observations in the flow field are supported by surface flow pictures.

In addition to the measurements numerical calculations have been made of the inviscid flow field about the cone, using a shock capturing technique proposed by Paul Kutler NASA-Ames.

ACKNOWLEDGEMENT.

The authors are very grateful to Mr. O.J. Anema for the efficient preparation of the computer program for reducing the data and for his assistance in obtaining the final results.

CONTENTS.

NOMENCLATURE.

F_1, F_2, F_3, F_4, F_5	functions describing properties of the five hole conical-head probe
M	Mach number
M_c	conical Mach number
n	power in the super-ellips formula
p_1, p_2, p_3, p_4	surface pressures of the probe
p_5	pressure measured by the central orifice
p_s	mean value of the surface pressures of the probe
Δp_α	pressure ratio $\frac{p_2 - p_1}{p_5}$
Δp_β	pressure ratio $\frac{p_4 - p_3}{p_5}$
R	local radius of the cone
u,v,w	velocity components in spherical coordinates
q	conical velocity
x,y,z	cartesian coordinates
α	angle of incidence
γ	slope of a conical streamline projected on a plane normal to the cone axis
ϕ_p	roll angle of the probe
θ	angle of pitch
θ_c	semi-apex angle
θ_p	angle of pitch of the probe

1. INTRODUCTION.

The investigation of the flow field about cones at high angles of incidence is of considerable interest, theoretically as well as experimentally. Numerical solutions have yielded good results for rather small angles of incidence, where no flow separation occurs and where one may consider the flow to be inviscid. In the present investigation we are concerned with the flow field about cones at high angles of incidence, of which, for the inviscid case, numerical results have been presented in Refs 1, 2, 3. At this high incidences, however, viscous effects play a dominant role, especially at the leeward side of the cone. The flow field is more complicated and numerical calculations of the inviscid flow field result only partially in an agreement with experiments. In 1963 Tracy (Ref. 4) showed for the first time the complexity of the flow field at high angles of incidence and after him several other investigators (Refs 5-11) confirmed the strong viscous-inviscid interaction at the leeward side of the cone. At angles of incidence even below the cone half-angle, crossflow separation was observed. At increasing incidences a system of counterrotating vortices developes in the separated region. Over a wide range of Mach numbers from low supersonic to hypersonic and for cone half angles ranging from about 5 deg. to 20 deg., the development of these phenomena are quite similar (see Refs 4-12).

Calculations of Lubard and Helliwell (Ref. 13) and Massot (Ref. 14), using an approximation of the steady-state Navier-Stokes equations lead to the formation of vortices in the separated zone. A reasonable agreement was found with Tracy's experiments. As may be expected that in the near future the interaction of viscous and inviscid flow will be calculated more accurately, a lot of experimental data will be needed to check theoretical results and to get a better understanding of these flow phenomena.

In the present report the measurements of the flow field about a cone at several angles of incidence are reported. One of the most important aims was to obtain a detailed impression of the velocity distribution

in the flow field; then, regions with flow separation and vortices will be clearly indicated by these velocity distributions. Also the regions of conical subsonic and supersonic flow will result. The experiments were performed, using a five hole conical-head probe, which measures the pitot pressure as well as the flow angularity. For the location of the embedded shock waves only the pitot pressure distribution was used. In addition to the flow field measurements also surface flow pictures have been made.

2. EXPERIMENTAL APPARATUS.

2.1. Test facilities.

The experiments were made in two supersonic blow-down wind tunnels of the University of Technology Delft, Department of Aerospace Engineering, the TST 27 and the ST 15, having test sections of 0.27 m x 0.27 and 0.15m x 0.15m, respectively. The TST 27 wind tunnel is equiped with a variable nozzle and operates in the Mach number range from M $\sim$ 0.5 up to M $\sim$ 5.5. The maximum value of the settling chamber pressure is 40 kg/cm^2. The TST 27 was used to provide surface flow visualization of the cone model at different angles of incidence and at different Mach numbers. Moreover, part of the schlieren pictures were made in this wind tunnel.

The flow field measurements have been made in the ST 15 wind tunnel, which has fixed nozzle blocks. The free stream Mach number, determined from pitot pressure measurements, had a mean value of 2.94 with local variations in the test section of less than 0.3%. During the measurements the settling chamber pressure was kept constant at a value of 5.45 $\pm$ 0.03 kg/cm^2. The specific humidity in the storage vessel for both wind tunnels was measured to be 0.86 x 10^{-4} kg/kg.

2.2. Models.

The model used for surface flow visualization in the TST 27 wind tunnel was a 7.5 deg. semi-apex angle cone. During the tests part of the cone surface was clad with a plastic sheet*. To avoid disturbances from the leading edge of the sheet a small backward facing step corresponding to the thickness of the sheet wase made in the cone surface 3.5 cm behind the cone apex. Moreover, a partition was made at the location of the step, so that the apex of the cone could be removed in order to be able to cover the cone surface with the sheet. In this way a smooth

---

* Fasson-Holland

composition could be obtained.
The model used in the ST 15 wind tunnel was a cone with a length of 15 cm and also a semi-apex angle of 7.5 deg. In test runs, preceding the actual measurements, strong irregularities in the flow field were observed. These were caused by very small, almost invisible deformations of the cone apex. A blunting of the apex appeared less disastrous and it hardly influenced the conical behaviour of the flow field. Therefore, the apex of the cone was carefully machined to avoid these disturbances.

2.3. Surface flow visualization.

To produce the surface flow patterns, a commonly used mixture has been applied, consisting of:

Shell Tellus 29 (oil)	30 grammes
Titanium dioxide	19 grammes
Shell T40 (detergent)	4 droplets

Instead of the use of oil-acid as a detergent, Shell T40 was chosen for its durability. After mixing the different parts in a gallipot, some steel balls were added and the whole was rotated during about 24 hours to get an ointment-like substance without real particles.
The plastic sheet covering the model was smeared with a thin layer of the oil-titaniumdioxide mixture. A satisfactory oil flow pattern was formed in about 20 seconds running time, depending on the Mach number of the flow. Due to the low temperature of the model after a run, the plastic sheet was very brittle. To be able to remove the sheet, the temperature was brought to room temperature (about $20^{\circ}C$). The temperature should not exceed about $35^{\circ}C$ in order to avoid deformations of the sheet and so of the streamline pattern. All oil flow patterns were photographed.

2.4. Conical-head probe (Fig. 1).

The measurements in the ST 15 wind tunnel were performed using a conical-head probe with a diameter of 3.5 mm and a semi-apex angle of 30 deg. The conical part of the probe was provided with four static pressure orifices with an angular displacement of 90 deg., moreover, a central orifice was fitted serving as a pitot pressure tap. The pressure orifices had a diameter of 0.3 mm, and the distance between two opposite holes was 1.54 mm. For these measurements the probe chosen was not the smallest available, but due to some ceramic dust in the wind tunnel air flow, the size of the probe was necessary to prevent strong influences of probe damages on the calibrations of the probe.

2.5. Calibration of the probe.

An extensive calibration of the conical-head probe provides the possibility to determine all local flow quantities if the total temperature of the flow is known. The flow angularity is related to the pressure differences across the two sets of opposite pressure orifices.These pressure differences, non-dimensionalized by the local pitot pressure, depend also on the local Mach number. To determine the local Mach number the ratio of the pitot pressure and the mean static surface pressure may be used. This ratio, however, is also a function of the angle of incidence of the probe and of its semi-apex angle. Especially, the sensitivity on variations of the semi-apex angle is very strong, which means that small convergencies or divergencies in the local flow field may lead to considerable errors in the Mach number measurements. Therefore, corrections to allow for these errors are necessary.

Another fact which may cause inaccuracies is the finite number of static pressure holes in the conical part of the probe, resulting in a mean value of the static surface pressure depending not only on the angle of incidence of the probe but on its roll angle as well. Considering the difficulties in interpreting the results of the measurements with a conical-head probe, the following calibration procedure has been chosen.

To calibrate the probe the TST 27 wind tunnel was used at three different Mach numbers, M = 2.2, M = 2.97 and M = 3.5. The execution of the three calibrations was similar. The probe was mounted on the variable pitch support. The five pressure orifices, a reference pitot probe and a total head probe in the settling chamber were connected with 7 calibrated Statham pressure transducers. At a particular Mach number the calibration of the probe was started with the two static pressure orifices 1 and 2 (see Fig. 1) in a vertical position, being in the plane in which the angle of incidence was varied. During one run the settling chamber pressure was kept constant and the angle of incidence of the probe was varied from -2 deg. up to 16 deg. with steps of one degree. At each step the output of the pressure transducers and of the digital indication of the angle of incidence was recorded in punch tape. The measurements were computer controlled and in behalf of the pressure measurements a "time-lag decision procedure" was built in in the computer program. Every next run was made with the pressure orifices rotated over an angle of 45 deg. with respect to the preceding position, up to a final value of 315 deg. This procedure was repeated for the two other Mach numbers. From the measured data several pressure functions were determined, such as the functions relating the pressure differences across opposite orifices to the angle of pitch θ:

horizontal $\dfrac{p_2-p_1}{p_5} = F_1(\theta)$ (1)

vertical $\dfrac{p_4-p_3}{p_5} = F_2(\theta)$ (2)

} at constant values of the Mach number M and the roll angle ϕ of the probe.

where p_1, p_2, p_3, p_4 are the surface pressures of the conical part of the probe and p_5 is the pressure measured with the axial orifice of the probe.

Due to the upwash and sidewash of the tunnel flow and due to imperfections of the probe, the functions $F_1(\theta)$ and $F_2(\theta)$ are different from zero at $\theta = 0$. A correction for the wind tunnel upwash and sidewash was obtained by calibrating the probe at roll angles ϕ and

ϕ + 180 deg. The remaining constants in $F_1(\theta)$ and $F_2(\theta)$ are attributed to probe imperfections.

The ratio of the mean value of the four static surface pressures and the pitot pressure is given, as a function of the Mach number, by:

$$\frac{p_1+p_2+p_3+p_4}{4p_5} = F_3(M)\Big|_{\theta_c = \text{const.}}^{\theta = 0} \tag{3}$$

This function is used for the determination of the Mach number. For the actual exploration of a flow field, functions of

$\Delta p_\alpha = \frac{p_2-p_1}{p_5}$ versus $\Delta p_\beta = \frac{p_4-p_3}{p_5}$ are used. For θ = constant these functions resemble ellipses having their axes along the Δp_α and Δp_β coordinate axes. To a very good approximation ($\Delta\theta$ = ± 0.1 deg.) these so called "super-ellipses" may be written as:

$$\left[\frac{\Delta p_\alpha - C_1}{F_1(\theta)-C_1}\right]^{n(\theta,M)} + \left[\frac{\Delta p_\beta - C_2}{F_2(\theta)-C_2}\right]^{n(\theta,M)} - 1 = 0 \tag{4}$$

where the power $n(\theta,M)$ is close to the value 2 and depends on the Mach number and the angle θ, the constants C_1 and C_2 deal with probe imperfections (curvature of the probe, mislocation of the static pressure orifices, etc.). As the pressure ratio $\frac{p_1+p_2+p_3+p_4}{4p_5}$ is not only a function of the Mach number but of the angle of incidence θ as well, the next function to be determined from the calibrations is:

$$\frac{p_1 + p_2 + p_3 + p_4}{4p_5} = F_4(\theta)_{M=\text{const.}} \tag{5}$$

It is used as a correction on $F_3(M)$. The local static pressure in the flow field will be determined from the Mach number and the local pitot pressure. Because the flow will generally be inclined to the probe, the measured pressure p_5 has to be corrected in order to obtain the pitot

pressure. So for each Mach number a function $F_5(\theta) = \frac{p_p}{p_5}$ must be determined from the calibrations.
With the functions F_1 to F_5 known and also the total temperature, all flow quantities may be determined from flow field measurements to a high degree of accuracy. For angles θ less than 20 deg. the influence of the circumferential angle ϕ on the correction function F_4 may be neglected. For $\theta > 20$ deg. the influence of ϕ must be taken into account, but during the actual measurements, the probe was mounted such that the maximum flow inclination with respect to the probe was less than 20 deg. at any place in the flow field.

2.6. Data acquisition.

2.6.1. Surface oil flow patterns.

Photographs were taken of the plastic sheets with the surface flow patterns, from which the direction of the local shear stress was measured. The accuracy of the readings was about half a degree.

2.6.2. Flow field measurements.

All data of the flow field measurements were recorded in punch tape. The pressures were measured by means of Statham pressure transducers, the settling chamber temperature was determined relative to melting ice with a thermocouple. The position of the probe in the symmetry plane of the cone at incidence was determined optically by two cathetometers, of which the readings were added separately to the punch tape. The displacement of the probe normal to the plane of symmetry of the cone was performed by a Slo-Syn stepping motor. The position of the probe was determined by counting the number of steps (0.015 mm per step) from a well defined reference point inside the testsection. The data reduction was done by the IBM 370/158 computer of the University.

3. DESCRIPTION OF THE TESTS.

Before the cone field measurements, the empty test section was calibrated mainly to locate pronounced disturbances in the flow. The position of the cone model was chosen such that no disturbances reached the plane in which the measurements were made. A second important point to know was the flow direction in the empty test section. Calibrations with the five-hole probe showed a down wash of about 0.2 deg. in the plane of measurement. The actual investigations were made in the flow field of a 7.5 deg. semi-apex angle cone at a Mach number of 2.94 and at incidences of 7.5, 12.4, 17.3, 22.4 and 25 deg. Although the cone was fixed at a certain incidence, a small increase in incidence occurred due to aerodynamic loads. For the sake of data reduction the angle of incidence was taken as the average value of about 10 optical measurements during preliminary runs. The deviation in the optical measurements was less than 0.02 deg.

An outline of the test arrangement is given in Fig. 1. The five-hole probe could not be mounted exactly parallel to the wind tunnel axis. Measurements indicated an angle of incidence of -0.33 deg. and a sweep angle of -0.19 deg. For these deviations corrections have been applied in the data reduction computer program.

The experiments were made in a plane normal to the wind tunnel axis, at about 125 mm downstream of the apex of the cone. The probe was traversed normal to the plane of symmetry with intervals of 1.51mm, being the latera distance between the central hole of the probe and one of the pressure taps on its conical surface. After each step the five probe pressures were read, together with the settling chamber pressure, the settling chamber temperature, a reference pitot pressure in the undisturbed part of the test section and the lateral position of the probe, the time-lag was taken into account at each step. The full traverses were made at levels with a relative vertical distance of the probe of about 1.5 mm. During each run the vertical position of the probe was measured optically with an accuracy of 0.03 mm. This reading was recorded into the punch tape after each traverse. To check the symmetry of the flow

field above the cone the traverses were started at 15 mm beyond the plane of symmetry. Each traverse was stopped about 6 mm after crossing the bow shock wave of the cone. Adjacent to the cone the measurements were started as close to the cone-surface as possible. In this way, at one angle of incidence the whole flow field was scanned by about 60 traverses with a maximum of 46 points each.

4. DATA REDUCTION.

The results of the measurements are presented in a spherical coordinate system. The origin of the system is situated in the apex of the cone, and one of the reference axes coincides with the cone axis. A reference plane is the plane of symmetry through the cone axis and the free stream velocity vector. In this system the three coordinates are r, ϕ and θ (Fig. 2). The components of the local velocity are u in radial direction, v in a meridional plane and normal to the local ray through the cone apex and w normal to u and v. The total component normal to a ray is called the conical velocity q. The conical Mach number M_c is defined as the ratio of the conical velocity and the local speed of sound.
In the flow field about the cone the local Mach number and the direction of the flow with respect to the probe axis have been determined from the probe pressures only. The Mach number results from the ratio of the pitot pressure, p_p, and the average value of the four cone surface pressure readings, p_s. As this ratio depends on the angle θ_p between the local velocity vector and the probe axis, the angle θ_p is calculated using the superellips relation, given by Eq. (4) which for $\theta = \theta_p$ reads:

$$\left[\frac{\Delta p_\alpha - C_1}{F_1(\theta_p)-C_1}\right]^{n(\theta_p,M)} + \left[\frac{\Delta p_\beta - C_2}{F_2(\theta_p)-C_2}\right]^{n(\theta_p,M)} - 1 = 0 \qquad (6)$$

The influence of the Mach number on θ_p is so small, that with this computed value of the angle θ_p the calculated Mach number is corrected adequately. Using this Mach number, θ_p is calculated once again with the super ellips relation. This value of θ_p is considered to be the last approximation.
The local static pressure has been determined from the Mach number and the measured pitot pressure, which has been corrected for the pitch angle θ_p. The local speed of sound has been derived from the Mach number and the settling chamber temperature, with the assumption of constant enthalpy in the wind tunnel flow.

The last quantity to be determined is the roll angle ϕ_p of the velocity vector, which follows from the approximation:

$$\phi_p = \tan^{-1}\left[\frac{\Delta p_\alpha}{\Delta p_\beta}\right] = \tan^{-1}\left[\frac{p_2-p_1}{p_4-p_3}\right] \tag{7}$$

To avoid inaccuracies in the results, as a consequence of the finite dimensions of the probe, an interpolation scheme was used to get the values of the four cone static pressures at each datum point at the location of the central pitot orifice. In this way also the influence of divergency of the flow on the calibration is eliminated, which may be considered as an extra advantage of the interpolation procedure.
Due to flow divergencies the apparent probe cone angle varies, resulting in a variation of the probe characteristics; particularly the determination of the local Mach number is rather sensitive on the apparent probe cone angle.
From the measured flow quantities and from the position and inclination of the probe with respect to the cone, the vectorial quantities u, v, w may be determined in the spherical coordinate system. Because of the conical nature of the flow field, it is convenient to analyse this kind of flow on a unit sphere having its centre in the origin of the conical field. On the unit sphere a conical streamline may be defined as a line which is at every point tangent to the conical velocity component (normal to a ray through the origin). The conical Mach number is calculated from the measured Mach number, the position of the probe and the direction of the local velocity vector, using the relation:

$$M_c = M\left[\sin^2\theta\sin^2(\phi-\phi_p)+\{\sin\theta\cos(\phi-\phi_p)\cos\theta_p-\cos\theta\}^2\right]^{\frac{1}{2}} \tag{8}$$

In order to be able to represent the data in a plane normal to the cone axis the velocity components are projected along rays through the origin by means of central projection. The position of a point on a unit sphere is found on the plane as the intersection of a ray through the point on the sphere and the origin.

The cartesian coordinates in the plane are non-dimensionalised by the local radius R of the cone cross-section in the plane.
The above mentioned central projection of the velocity components implies the possibility of tracing the conical streamlines in the plane normal to the cone axis. Then, the slope of the streamlines in the plane is given by:

$$\tan\gamma = \frac{\sin\theta\cos\phi - \frac{z}{R}\cos\theta\tan\theta_c}{\sin\theta\cos\phi - \frac{y}{R}\cos\theta\tan\theta_c}$$

where γ is the angle with the positive y-axis.

5. RESULTS.

5.1. Surface flow.

In Fig. 3 photographs of the surface flow patterns are given. The line of symmetry represents the leeward side of the cone and the straight edges form the windward side. At an angle of incidence α = 6 deg. no special features can be observed. If the angle of incidence is increased up to 10 deg. (Fig. 3a) a narrow region occurs at either side of the symmetry plane where the oil flows together; this may be a first indication of flow separation. Simultaneously a reattachment of the flow appears at the leeward symmetry plane, giving evidence of the development of a symmetrical vortex system. At α=12 deg. (Fig. 3b) the separation zone inclines to reduce to a sharp line. Also a second separation line may be observed, which indicates a secondary vortex system within the first region of separated flow. At α = 14 deg. the flow is fully developed to a flow with sharp separation lines (Fig. 3c). This flow structure holds, up to an incidence of about 26 deg. (Fig. 3d). A qualitative sketch derived from the surface flow visualizations is given in Fig. 4. The location of the separation and attachment lines as a function of the angle of incidence has been drawn in Fig. 5. At small incidences the separation lines are both at a circumferential angle ϕ of about 160 deg. At increasing angle of incidence the position of the second separation is not changed, the primary separation, however, moves to ϕ = 120 deg. approximately, probably due to the growth of the secondary vortex system. This is in agreement with Ref. 15. At incidences exceeding 25 deg. the position of the primary separation changes again to a circumferential angle which is closer to the leeward symmetry plane.

Houwink (Ref. 12) showed the existence of non-symmetrical effects at angles of incidence exceeding 28 deg. This might influence the position of the separation lines at somewhat smaller incidences.

In Fig. 6 the measured direction of the shear stress at different angles of incidence is given as a function of the circumferential angle; here, u is the velocity component along a generator of the cone, and w the

velocity component in circumferential direction. Due to the absence of a pressure gradient along a generator of the cone, the secondary flow in the sublayer of the boundary layer is dominated by the circumferential pressure gradient. So the angle of the surface streamlines with respect to a generator will be larger than in the inviscid case. Figs 6a and 6b show the measured shear stress distribution compared with the values from Ref. 16 at incidences of 6 and 8 deg. respectively. No separation was observed up to α = 8 deg. At α = 10 deg. a first separation occurs (Fig. 6c), followed, at α = 12 deg. by a secondary separation and a reattachment zone (Fig. 6d). The abrupt changes in the direction of the shear stress at α = 14 deg. (Fig. 6e) may indicate the existence of an embedded shock wave standing on the cone surface at $\phi \tilde{\sim} 120$ deg. In this range of incidences (α = 12-14 deg.) the flow may be said to be in a state of transition from a structure which depends strongly on the incidence, into one which is almost independent of α. For values of α larger than 14 deg. approximately, a flow structure with several pronounced separations and attachments occurs. Increasing the angle of incidence still further one might observe that the surface flow structure does not change until $\alpha \tilde{\sim} 26$ deg. (Fig. 6g). It seems that the embedded shock wave stabilises the flow structure up to that angle of incidence. In Fig. 6f the direction of the shear stress, as calculated for inviscid flow using a shock capturing technique, is given for α = 17.3 deg. The direction of the shear stress changes abruptly at $\phi \tilde{\sim} 150$ deg., just where the shock wave appears in the computed inviscid flow field. Although there is some agreement in the inviscid and viscous results with respect to the shock wave, the entire flow structure of both is completely different, as will be seen later (Figs 21-22).

5.2. Flow field.

5.2.1. Pitot pressure distributions and flow directions.

In Fig. 7 lines of constant pitot pressure (non-dimensionalised by the free stream total pressure) are given at α = 12.4 deg. No regions of strong gradients are observed; however, near the plane of symmetry and in the neighbourhood of the cone surface there exists a slightly steeper decrease in pressure.

The pitot pressure in the leeward plane of symmetry, given in Fig. 8 for α = 12.4 deg., is rather constant up to a small distance from the cone surface. The decrease in pitot pressure may indicate an acceleration of the flow. At α = 17.3 deg. the pitot pressure distribution in the flow field is of a more pronounced nature (Fig. 9) than that at α = 12.4 deg. At the leeside, the isobars surround a region of very low pitot pressure. The pressure gradients of this region may be easily observed with a schlieren system. At a circumferential angle of about 125 deg., wiggles in the isobars indicate the existence of shock waves. The solid line in Fig. 9 certainly represents a shock wave, the shock wave indicated by the dotted line is less distinct. Together they form a lambda shock wave, which is a well known phenomenon in supersonic separated flows. As shown in Fig. 10 the pitot pressure in the leeward plane of symmetry is still very constant, again with exception of the part just above the cone surface, where a pressure decrease occurs.

At an angle of incidence of 22.4 deg. the low pitot pressure region clearly has developed into a pressure field similar to that of a vortex core, Fig. 11. The pitot pressure in the centre of the region of concentric isobars is very low with a minimum value of p_p/p_{t_∞} of about 0.07. The question arises whether it is possible to have a conical vortex in the flow field, e.g. a vortex satisfying the conditions for conical flow, which in turn implies that the vortex strength depends linearly on the distance to the conical centre. The present measurements give no decisive answer and more research is required to answer this question.

The embedded shock waves are now located at an circumferential angle of about 143 deg. The lambda structure still exists, but a new feature shows up. At α = 17.3 deg. the shock wave given as a solid line is slightly curved. For α = 22.4 deg. the shock wave is curved as well, but half-way a strong change in the direction may be seen, however, no sudden change can be found in the measured flow direction (Fig. 19). Moreover, Fig. 23 shows that the strong curvature of the shock wave is located at the intersection with a streamline, which divides the flow field into two regions, one that may be considered inviscid and the other is dominated by vortex flow. This supports the suggestion that the upper and lower parts of the shock wave are of different origin. The lower part may be generated by the flow separation from the cone surface, whereas the upper part is necessary to satisfy the boundary conditions in the inviscid flow. Both parts smoothly merge into each other. The upper part of the flow field may be found by computing the flow about a conical body having a cross section of which the leeward part is enclosed by the above mentioned dividing streamline. This has been done more or less in Refs. 11 and 17.

In the leeward plane of symmetry the pitot pressure gradients are strong in the vicinity of the cone surface, Fig. 12. The gradual decrease in pitot pressure starting at about $\frac{z}{R}$ = 2.7 continues in a rapid decrease at about $\frac{z}{R}$ = 1.7 and is followed by a sharp rise at $\frac{z}{R}$ = 1.25. The latter position agrees very well with the position of the shock wave just above the cone surface as may be observed in the schlieren photograph, Fig. 13. A more detailed impression of the pitot-pressure distribution in the leeward plane of symmetry is shown in Fig. 14, where a measurement with a small flattened pitot probe is given. This measurement has been made at a slightly smaller angle of incidence but the distribution is the same. At $\frac{z}{R}$ = 1.2 the shock wave has been measured as a jump in the pitot pressure, this in contrast with the rather wide spread measurements of Fig. 12.

The conical velocity distribution, measured at an angle of incidence of 12.4 deg., is given in Fig. 15. In this figure the arrows are all

of equal length, and therefore the length is not a significant measure for the magnitude of the conical velocity.

Linearised inviscid flow calculations (Ref. 18) result in a conical stagnation point away from the cone surface, the measurements also show a stagnation point, although it is not lifted off from the body. The measured conical velocity in the leeward symmetry plane, Fig. 16, is in agreement with the flow structure of Fig. 15, in that the conical velocity normalised by the local speed of sound is always less than zero; consequently no conical stagnation points away from the cone surface are measured.

It may be observed from Fig. 17 that at α = 17.3 deg. the flow structure has not changed essentially, compared to the flow at α = 12.4 deg. The conical stagnation point is still located on the cone surface. As suggested in Ref. 19 the strength of the leeward vortices is apparently of great influence on the appearence of conical stagnation points in the flow field. Even at relative large angles of incidence no conical stagnation points are observed away from the cone surface. For inviscid flow numerical calculations predict a conical stagnation point lifted off from the body surface, see Fig. 18, where also the measured data have been presented. It appears that the calculated stagnation point is formed well below the intersection of the free stream velocity vector with the $\frac{z}{R}$ axis (cone apex in Fig. 18). The measured values of $\frac{v}{a}$ remain negative. At an angle of incidence of 22.4 deg., Fig. 19, the flow field has changed into one with a separated stagnation point and a fully developed vortex system near the plane of symmetry. In addition a near-wake stagnation point has been formed at a $\frac{z}{R}$ value of about 1.9. In this point the dividing streamline terminates.

The strong change in flow direction appearing in the neighbourhood of the cone surface at the leeward side suggests a region of flow separation which is also observed in the oil flow patterns. In the plane of symmetry the conical velocity $\frac{v}{a}$ assumes twice the zero value, Fig. 20. Near the cone surface the velocity increases up to Mach numbers greater than one ($\frac{v}{a} < -1$). As we have seen already, the deceleration towards

the cone surface occurs in part by a shock wave. Due to the interference of the conical-head probe with the cone surface the flow direction measurements in the vicinity of the cone surface were not accurate. The shock wave across the symmetry plane was measured with a special pitot probe (Fig. 14) and was also observed on a schlierenpicture, Fig. 13.

5.2.2. Embedded shock waves and the distribution of the conical Mach number.

At an angle of incidence α = 12.4 deg. no embedded shock waves are found. The flow field between the bow wave and the cone appears to be conical subsonic. At α = 17.3 deg. the flow contains a conical supersonic region (Fig. 21), which is enclosed partly by a conical sonic line and partly by a lambda type shock wave. Downstream of the shockwave a second supersonic region has been measured, which we do not quite understand, because the supersonic pocket terminated by the embedded shock wave seems to be comparable with the plane transonic problem where no such region is observed to that extent. The occurrence of anomalies in the measurements is rather unlikely, because at higher incidences this second supersonic region is much larger and it seems to be a fundamental part of the flow field.

The results of a numerical calculation of the flow field using Kutler's shock capturing technique (Ref. 2) at the same angle of incidence are given in Fig. 22. The supersonic regime is more extended and the region of the shock wave is situated closer to the plane of symmetry than shown by the experiments. Downstream of the shock wave no second supersonic region was found. It is obvious that the development of a vortex near the plane of symmetry has a strong influence on the nature of the flow field and that in numerical calculations viscous effects have to be taken into account.

Fig. 23 shows the results of the measurements at α = 22.4 deg. This figure bears qualitatively a strong resemblance with the results obtained at α = 17.3 deg. (Fig. 22), however, the conical supersonic regime is much larger.

Also a third supersone regime is measured extending across the symmetry plane just above the cone. As usual, looking downstream along the conical streamlines, the region begins with a conical sonic line and ends with a shock wave normal to the symmetry plane. In the schlieren picture of Fig. 13 the shock wave is shown as a very straight line emanating from the cone apex; this suggests that the flow phenomena connected with the vortices are of conical character.

6. CONCLUDING REMARKS.

Because of the detailed flow direction measurements using a carefully calibrated probe, the investigation described in this report yields an extension of the information obtained so far on the viscous flow about circular cones. The existing knowledge of such a complex subject is mainly produced by experimental work, although for moderate angles of incidence the analyses of Lubard & Helliwell (Ref. 13) and of Bontoux and Roux (Ref. 20) show that very adequate numerical methods are developed to describe such a flow field. For large angles of incidence ($\alpha > 2\theta_c$) no theoretical results exist for the viscous flow, in particular the complex vortex system as given in the present report causes large difficulties.

In general the results of the underlying measurements agree very well with those of Refs. 6, 9, 10 and 12. The extension given in this report concerns the determination of conical supersonic regions, conical sonic lines, and of detailed flow directions.

At high angles of incidence the inviscid-viscous flow interaction at the leeward side of the cone causes an embedded shock wave with a peculiar shape not observed before, as far as known to the authors. In addition the measurements undoubtly show the existence of leeward vortices. Nevertheless, the streamline pattern in the very vicinity of the vortex core is only indicative because of the size of the probe. Therefore refined measurements are necessary to obtain a better information about the precise structure of the vortex core and of the existence of secondary vortices, which are only detected by the surface oil flow visualizations.

Although the main purpose of the present measurements has been the investigation of the flow field away from the cone surface, it will be clear now that precision surface pressure measurements are necessary to achieve a complete impression of the flow about the cone. From the literature it appears that at high angles of incidence the surface pressure results reveal considerable differences when comparing various contributions. Together with the refined flow direction measurements

mentioned above, also a careful attention will be given to a fine-interval determination of the surface pressure distribution.

REFERENCES.

1. Holt, M., Ndefo, D.E. — A Numerical Method for Calculating Steady Unsymmetrical Supersonic Flow Past Cones, Journal of Computational Physics, Vol. 5, 1970, pp. 463-486.

2. Kutler, P., Lomax, H. — A systematic development of the supersonic flow fields over and behind wings and wing-body configurations using a shock-capturing finite-difference approach, AIAA 9th Aerospace Science Meeting, New York, January 25-27, 1971, Paper No. 71-99.

3. Fletcher, C.A.J. — GTT method applied to cones at large angles of attack. Proceedings of the 4th International Conference on Numerical Methods in Fluid Dynamics, edited by R. Richtmyer, Lecture Notes in Physics, Vol. 35, Springer-Verlag, West Berlin, 1975.

4. Tracy, R.R. — Hypersonic Flow over a Yawed Cone, Graduate Aeronautical Laboratories California Institute of Technology, Pasadena, Memorandum no. 69, 1963.

5. Guffroy, D., Roux, B., Marcillat, J., Brun, R., Valensi, J. — Etude théoretique et expérimentale de la couche limite autour d'un cône circulaire placé en incidence dans un courant hypersonique. AGARD CP-30, Hypersonic Boundary Layers and Flow Fields, paper no. 20, 1968.

6. Rainbird, W.J. — The external flow field about yawed circular cones. AGARD CP-30, Hypersonic Boundary Layers and Flow Fields, paper no. 19, 1968.

7. Yahalom, R. — An experimental investigation of supersonic flow past yawed cones. Aeronautical Sciences Division University of California, Berkeley, 1971. (AFOSR-TR-71-2183)

8. Stetson, K.F. — Boundary layer separation on slender cones at angle of attack. AIAA Journal, Vol. 10 no. 5, May 1972. pp. 642-648.

9. Feldhuhn, R.H., Winkelmann, A.E. — Separated flow phenomena on a slender cone at Mach 5. NOL-TR-69-36, March 1969.

0. Feldhuhn, R.H., Winkelmann, A.E., Pasiuk, L. — An experimental investigation of the flow field around a yawed cone. AIAA paper no. 70-766.

1. Zakkay, V., Alzner, E. — Leeside flow field description over cones at large incidence. AFFDL-TR-74-19, 1974

2. Houwink, R. — Measurements at the leeward side of a cone at large incidences in supersonic flow. Delft University of Technology, Report VTH-186 1974.

3. Lubard, S.C., Helliwell, W.S. — Calculations of the flow on a cone at high angles of attack. AIAA paper no. 73-636.

4. Massot, P. — Détermination de quelques caracteristiques de la couche limite tridimensionelle turbulente autour d'un cône a M_∞=5. Thèse de Doctorat de Specialité Université d'Aix-Marseille.

15. Orlik - Rückemann, K.J., LaBerge, J.G., Iyengar. Half- and Full-Model Experiments on Slender Cones at Angles of Attack. JSR, Vol. 11, No 9, pp.575-580, September 1973.

16. Jones, D.J. Tables of Inviscid Supersonic Flow About Circular Cones at Incidence $\gamma = 1.4$. AGARDograph 137.

17. Nakao, S.I. Supersonic flow past conical bodies at large angles of attack. ISAS Report no. 534, Nov. 1975.

18. Bakker, P.G., Bannink, W.J. Conical Stagnation Points in the Supersonic Flow Around Slender Circular Cones at Incidence. Report VTH-184, 1974 Delft University of Technology.

19. Houwink, R., Nebbeling, C. Experimental investigation of the leeward flow field of a cone at high incidence in supersonic flow. Delft Progress Report, Series C,1(1975) pp. 69-76.

20. Bontoux, P., Roux, B. Compressible turbulent boundary layer on a yawed cone. AIAA Paper No. 75-858, 1975.

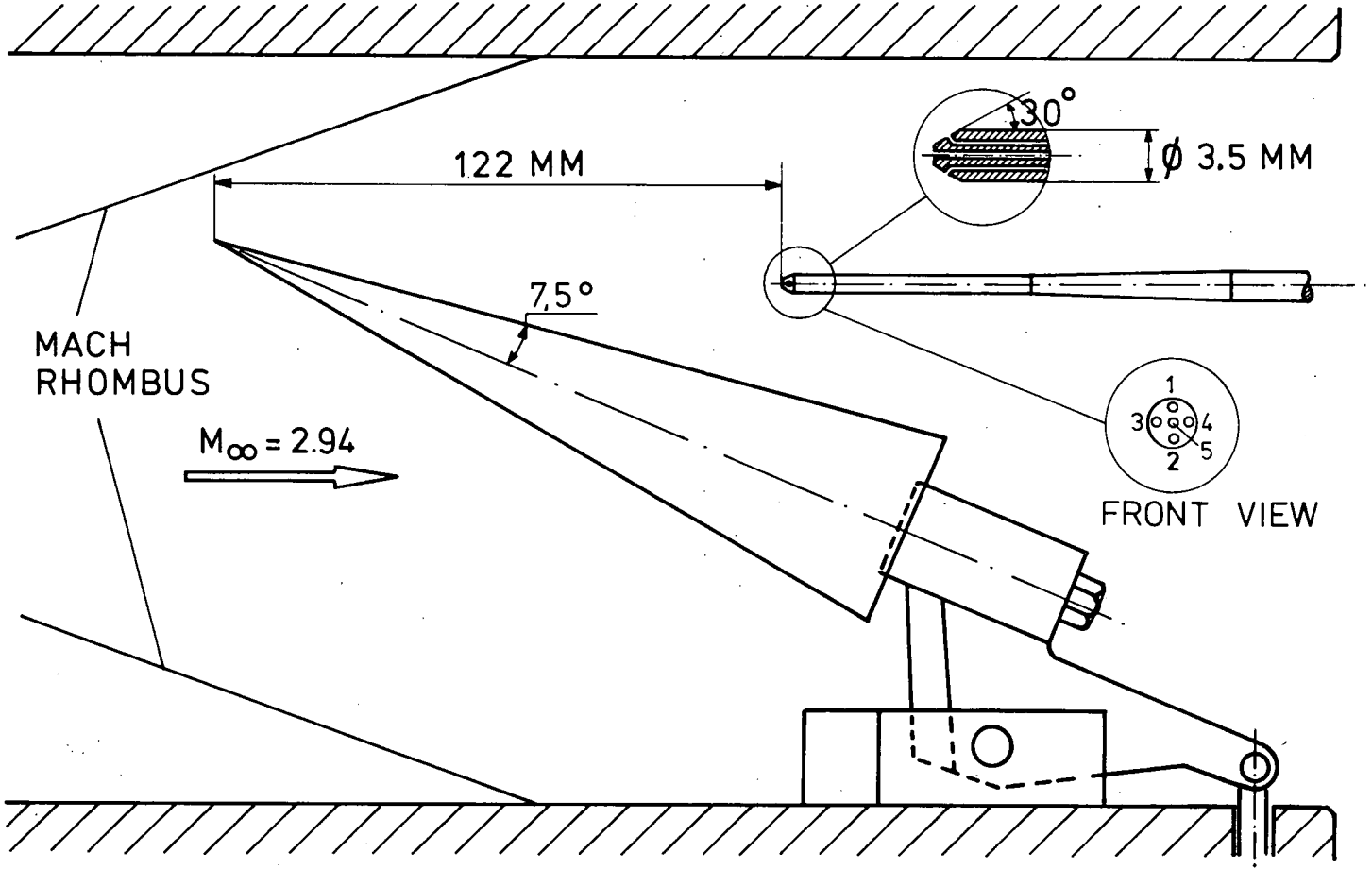

FIG .1: TEST ARRANGEMENT.

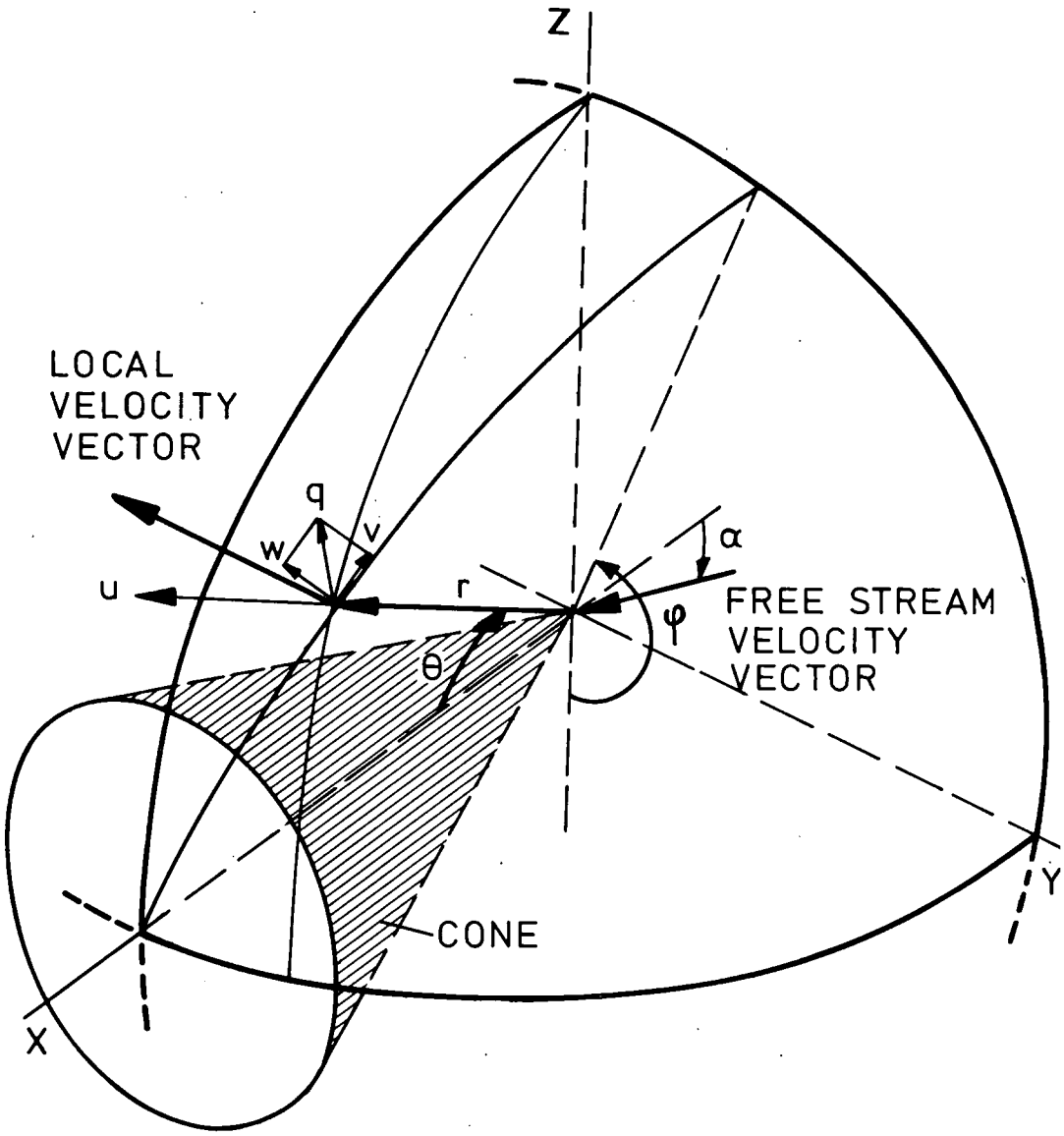

FIG. 2: SYSTEM OF CONICAL COORDINATES AND VELOCITY COMPONENTS.

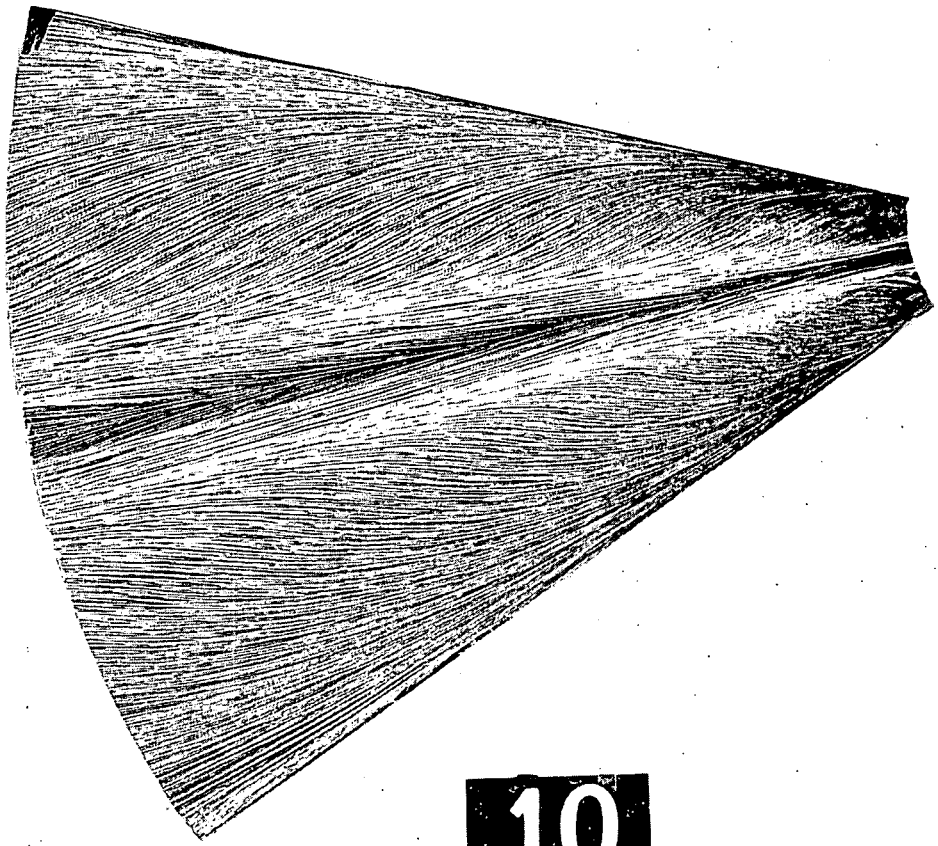

FIG. 3a : SURFACE FLOW PATTERN AT
$\alpha = 10$ DEG. $M = 2.94$ $\theta_C = 7.5$ DEG.

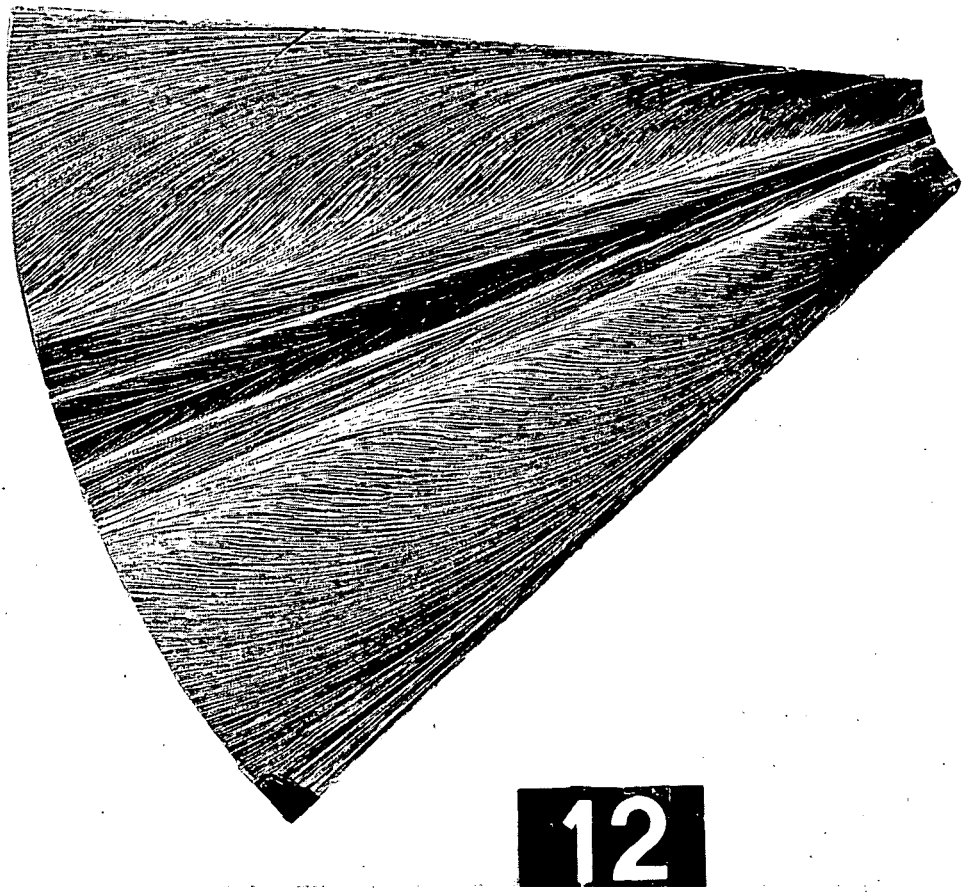

FIG. 3b: CONTINUED $\alpha = 12$ DEG.

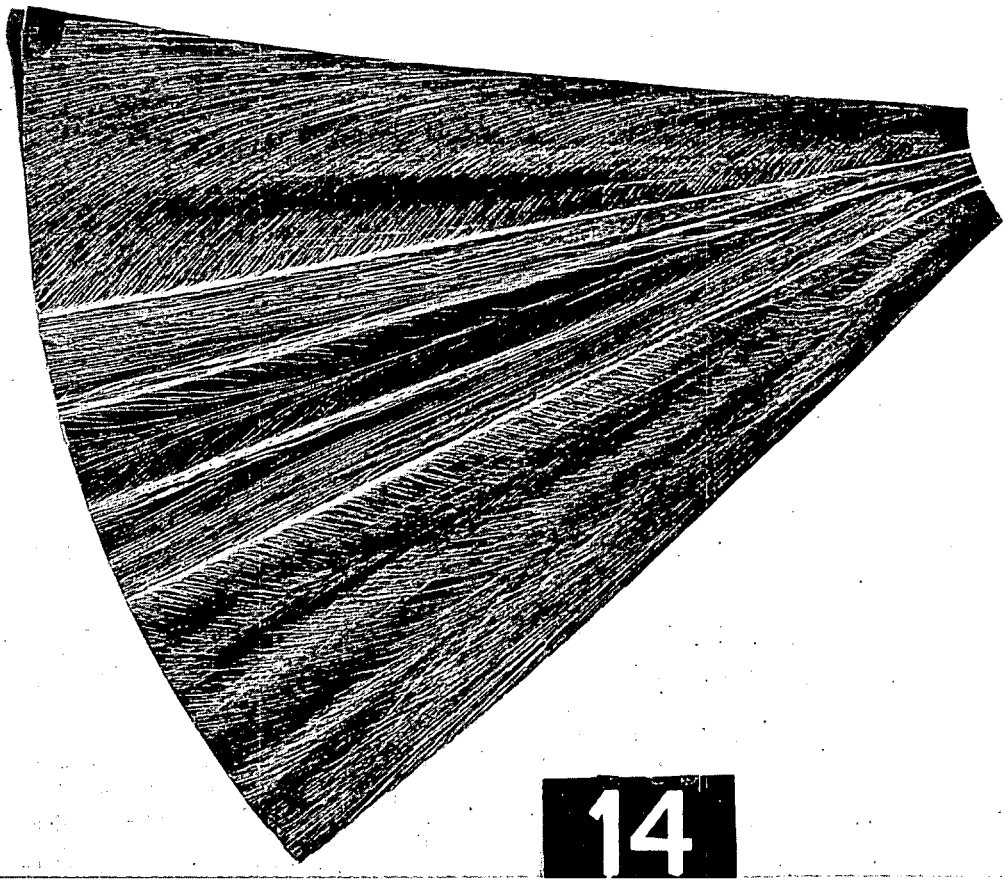

FIG. 3c : CONTINUED $\alpha = 14$ DEG.

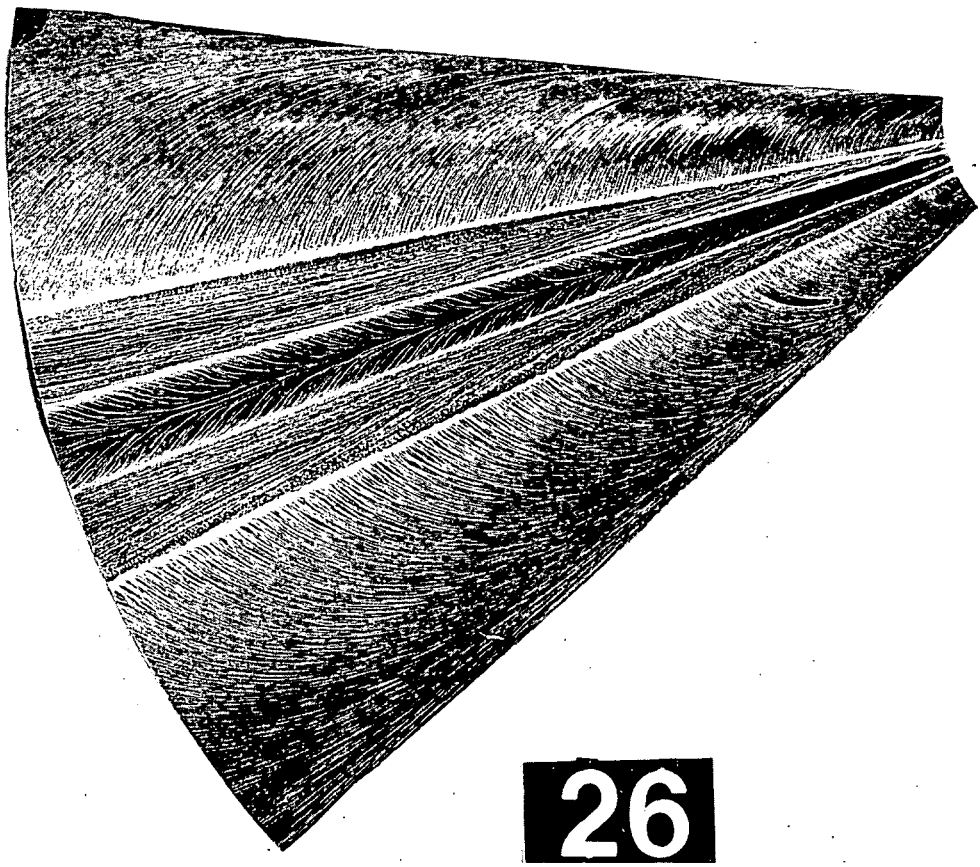

FIG. 3d : CONCLUDED $\alpha = 26$ DEG.

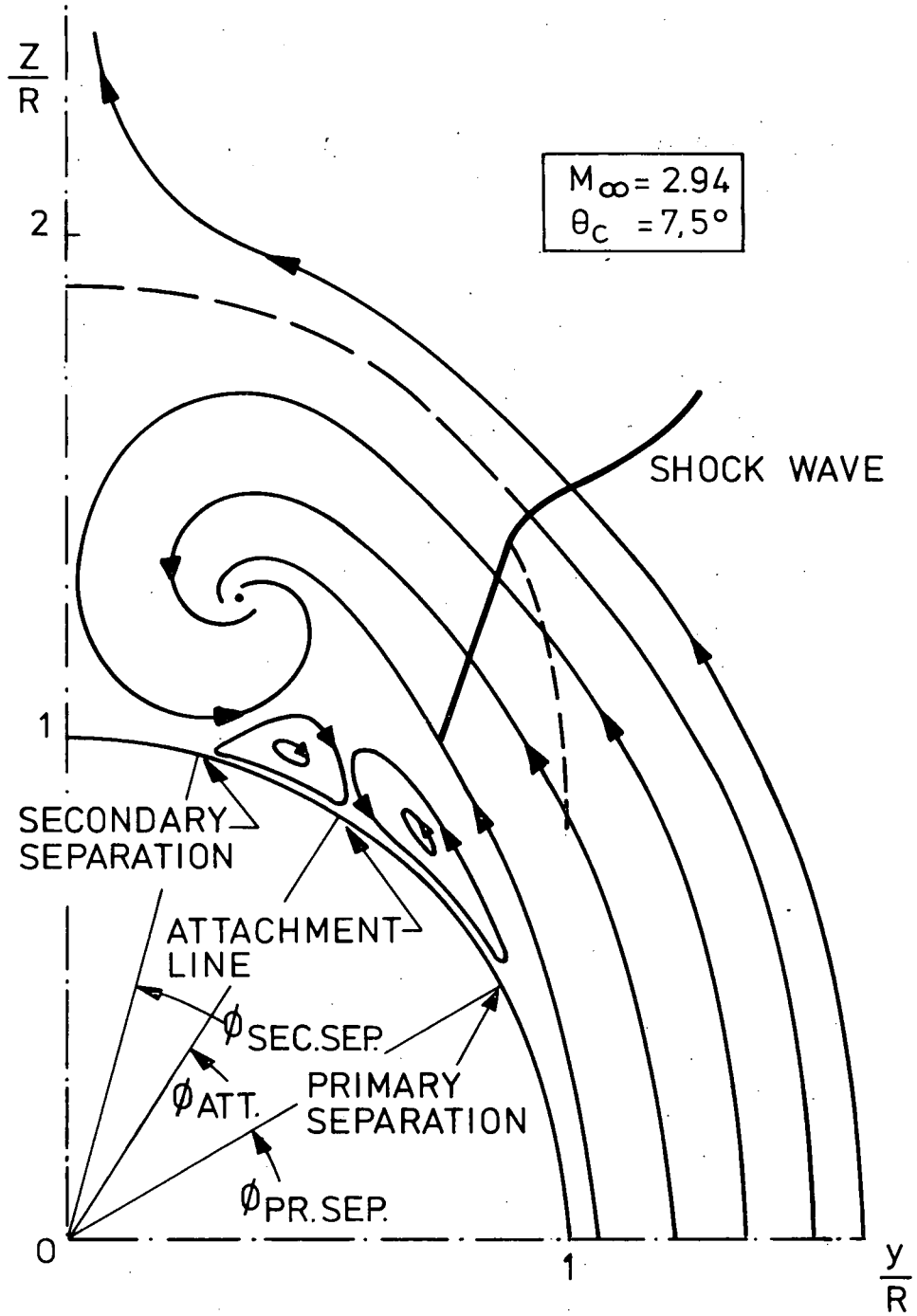

FIG .4 : POSSIBLE VORTEX STRUCTURE FROM SURFACE FLOW PICTURES AT α >12 DEG.

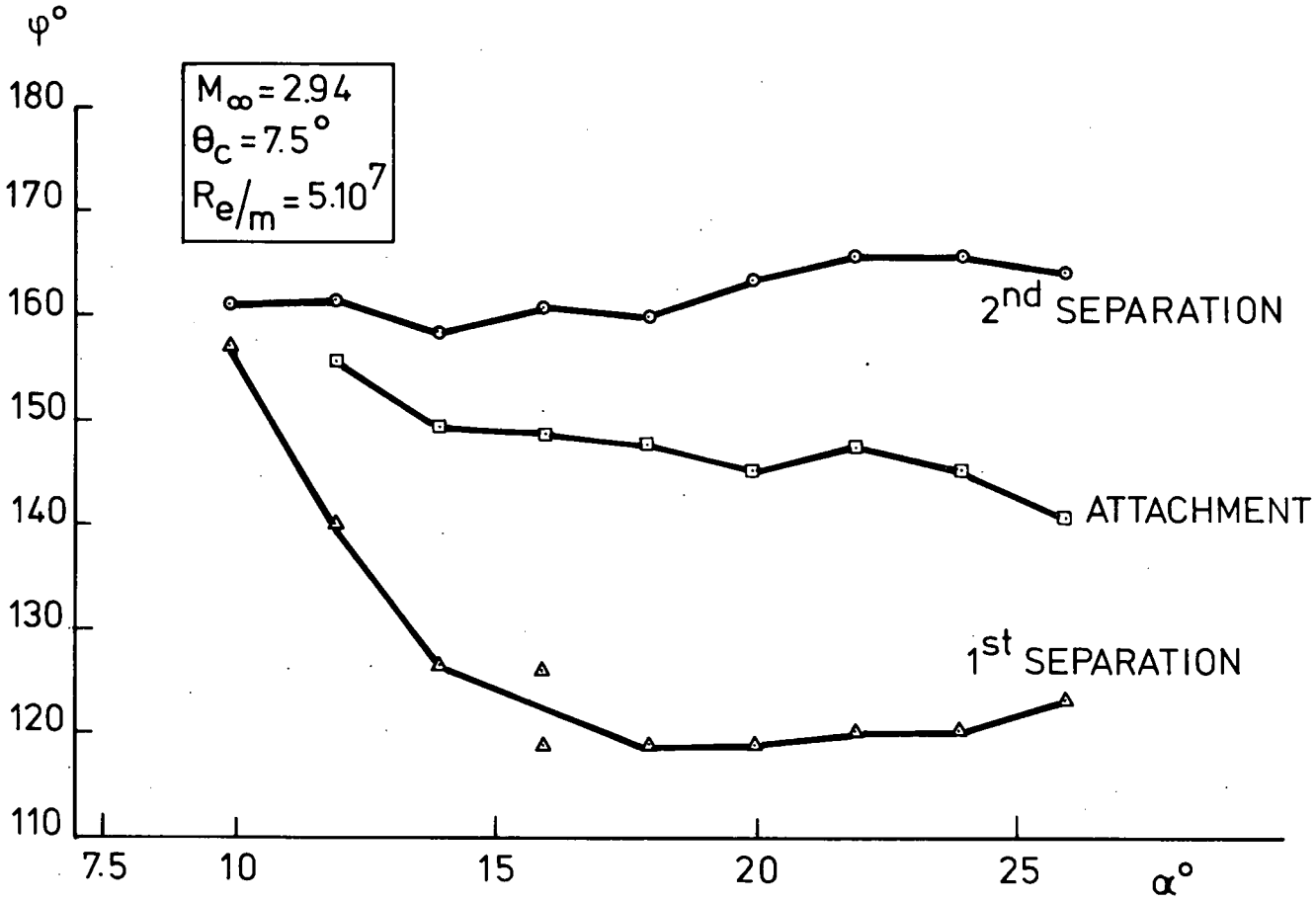

FIG. 5 : MERIDIONAL POSITION OF FLOW SEPARATION AND ATTACHMENT LINES.

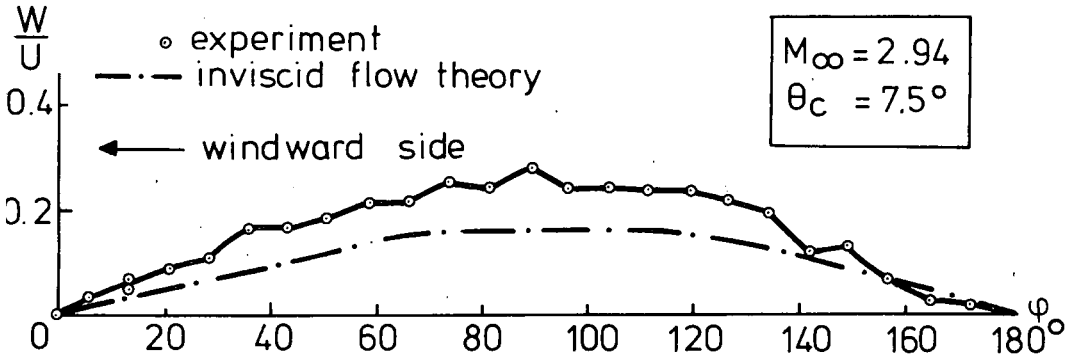

FIG. 6a: STREAMLINE DIRECTION ON THE CONE
$\alpha = 6$ DEG.

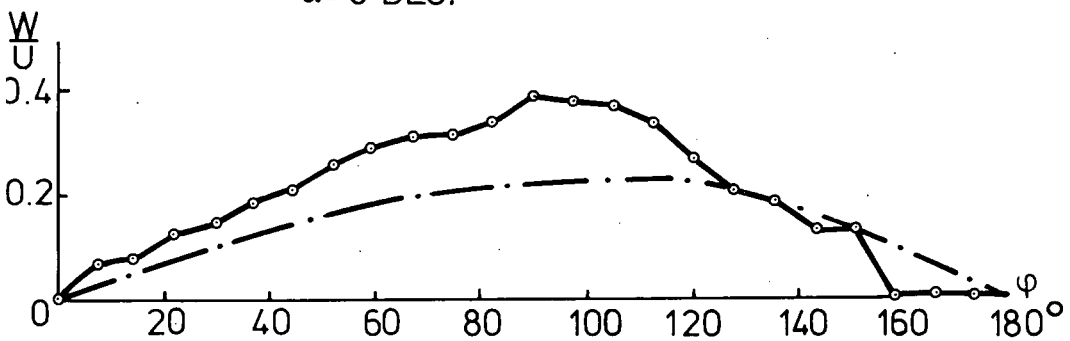

FIG. 6b: CONTINUED $\alpha = 8$ DEG.

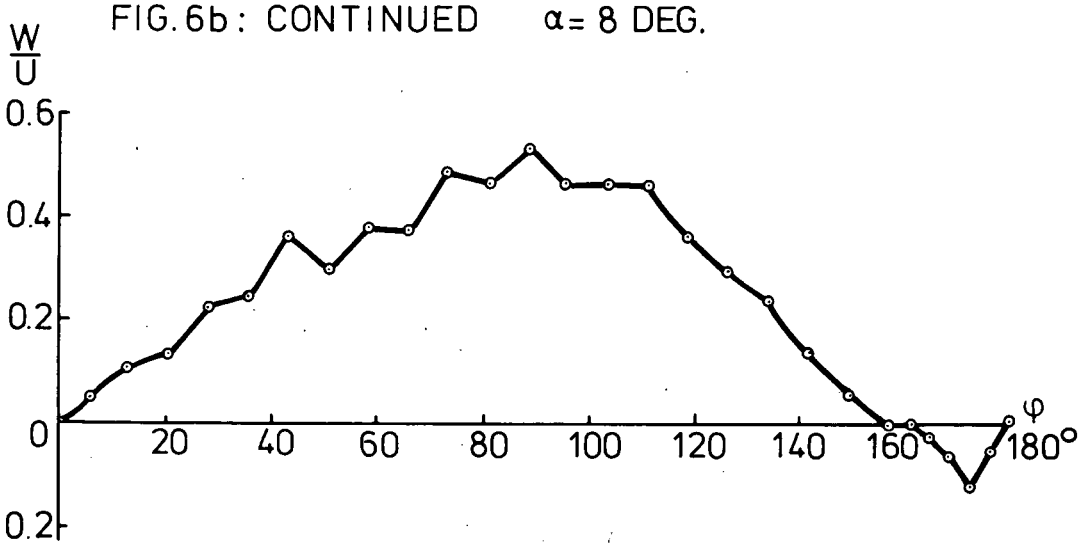

FIG. 6c: CONTINUED $\alpha = 10$ DEG.

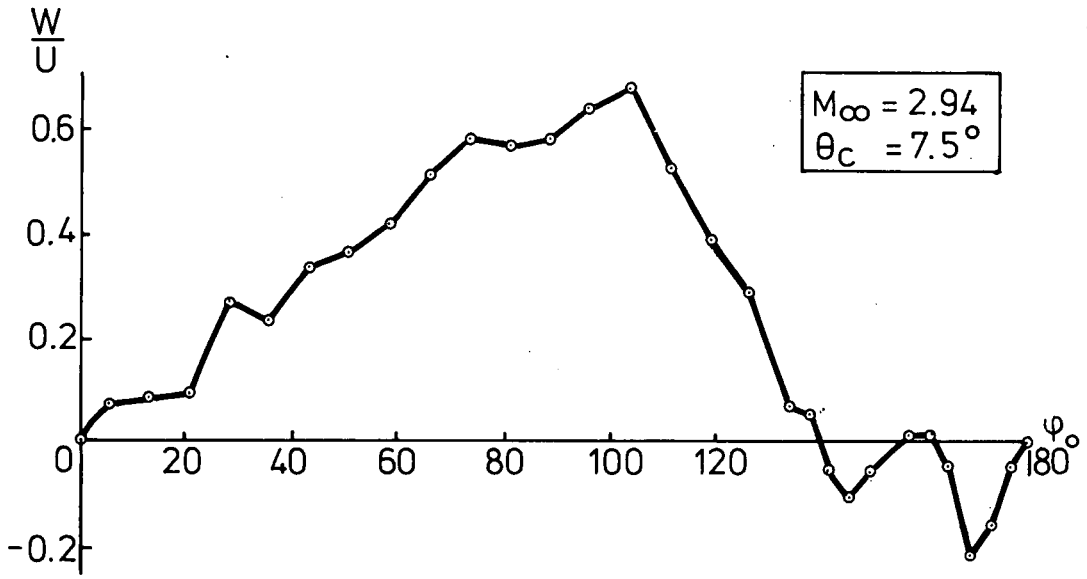

FIG. 6d: CONTINUED α = 12 DEG.

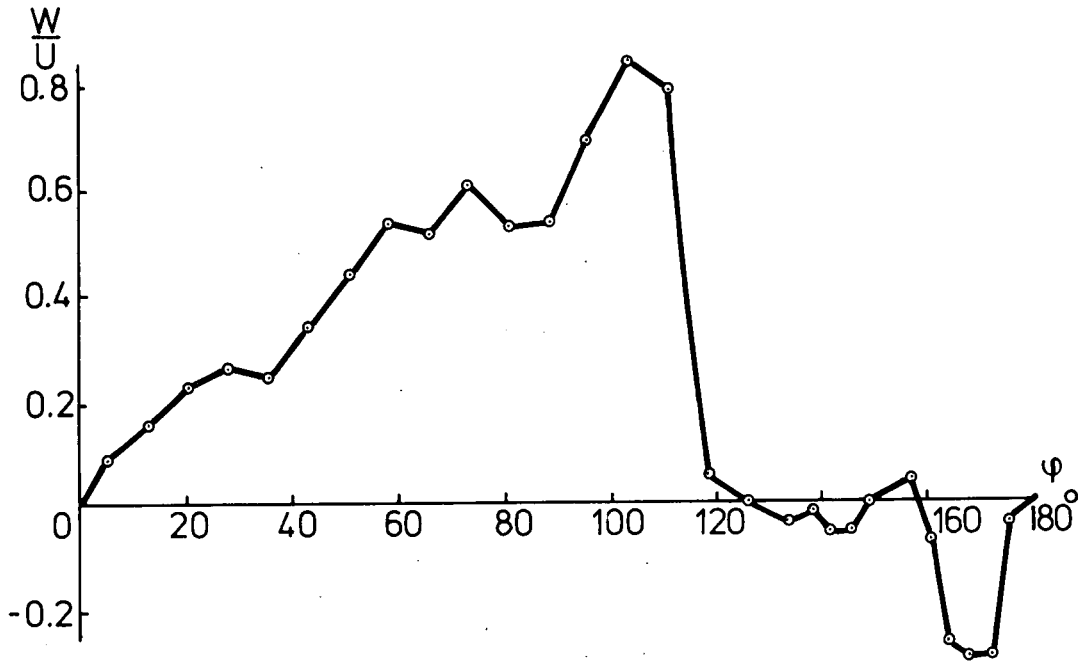

FIG. 6e: CONTINUED α = 14 DEG.

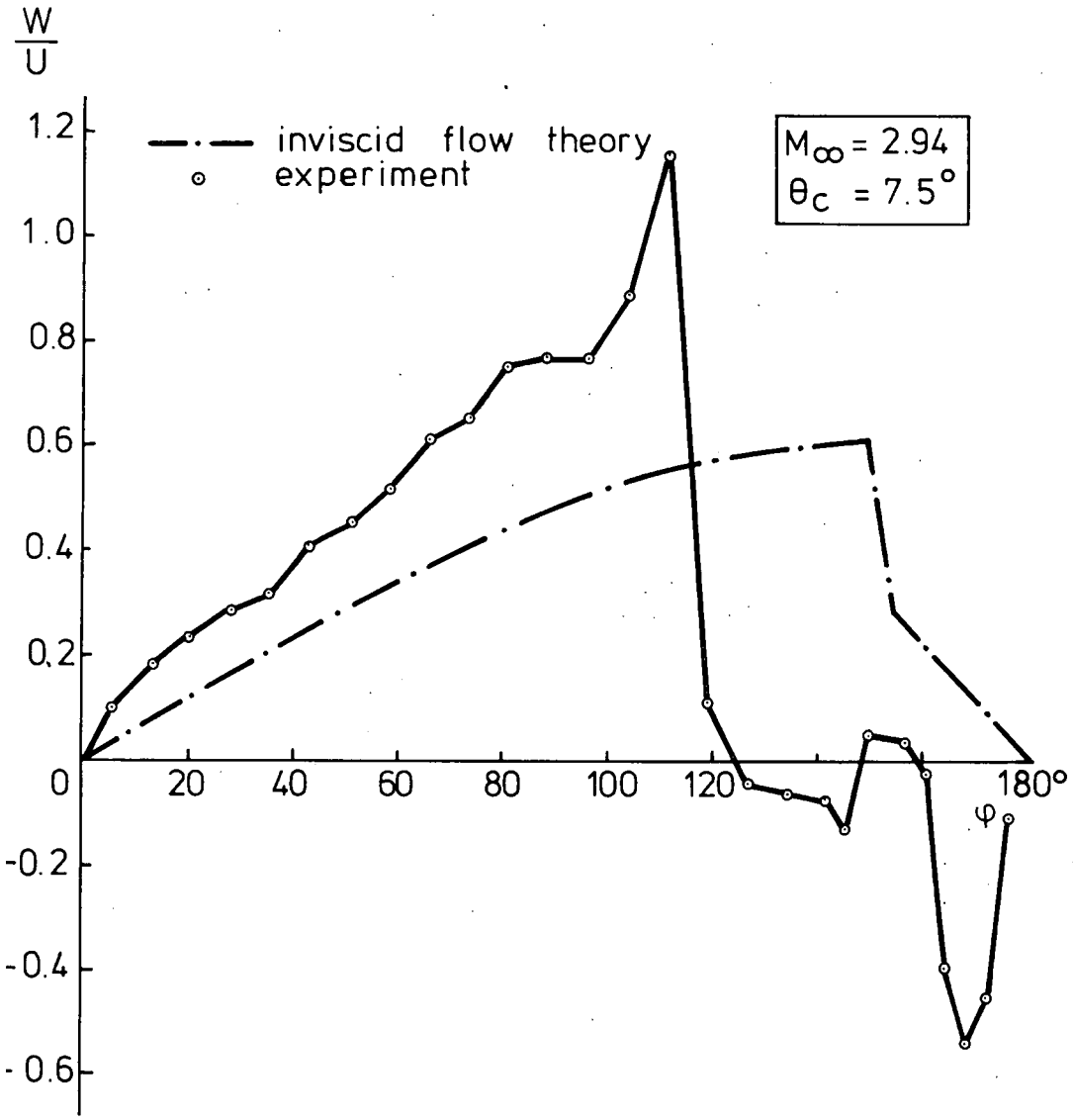

FIG. 6f : CONTINUED $\alpha = 17.3$ DEG.

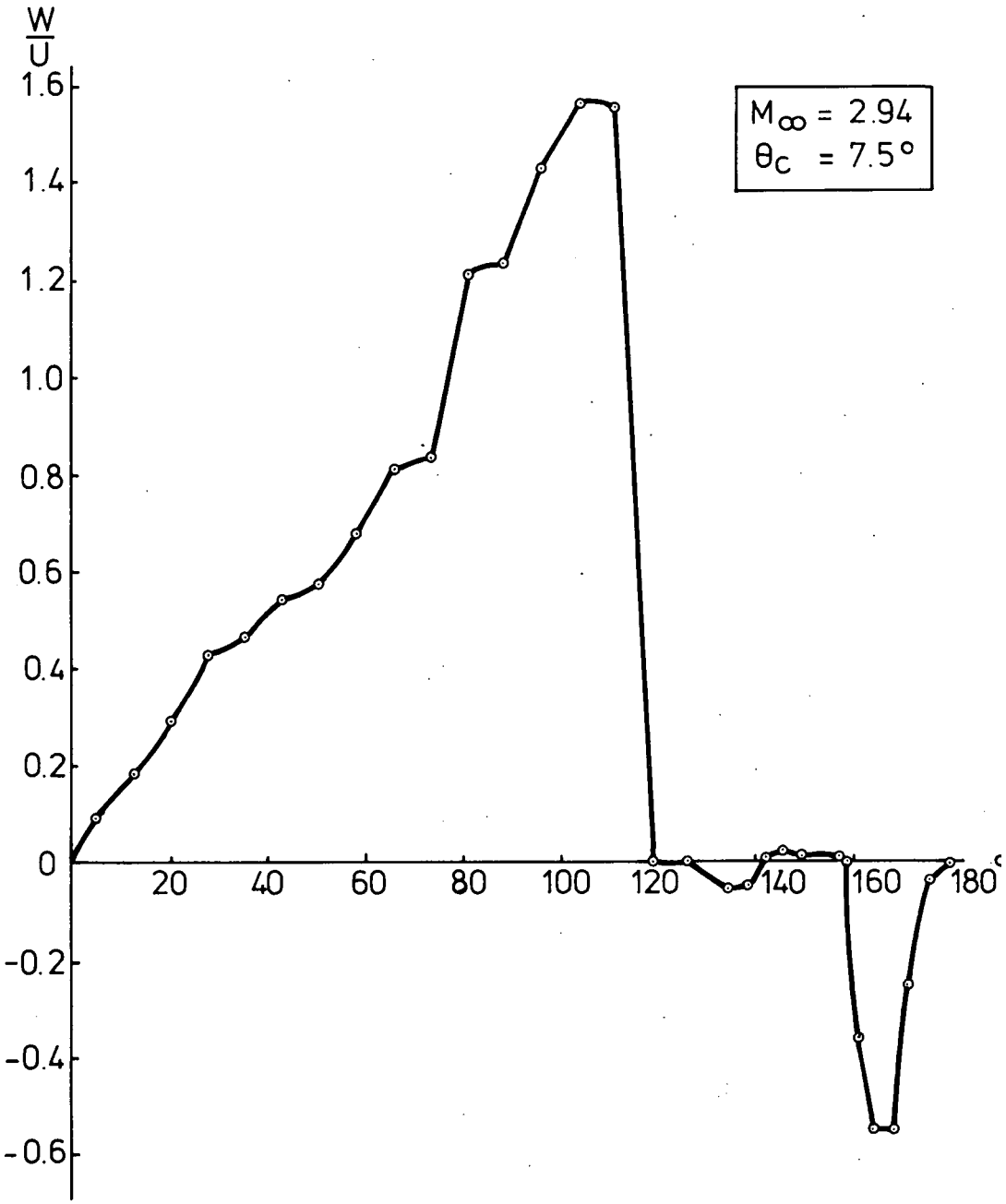

FIG. 6g : CONCLUDED $\alpha = 26$ DEG.

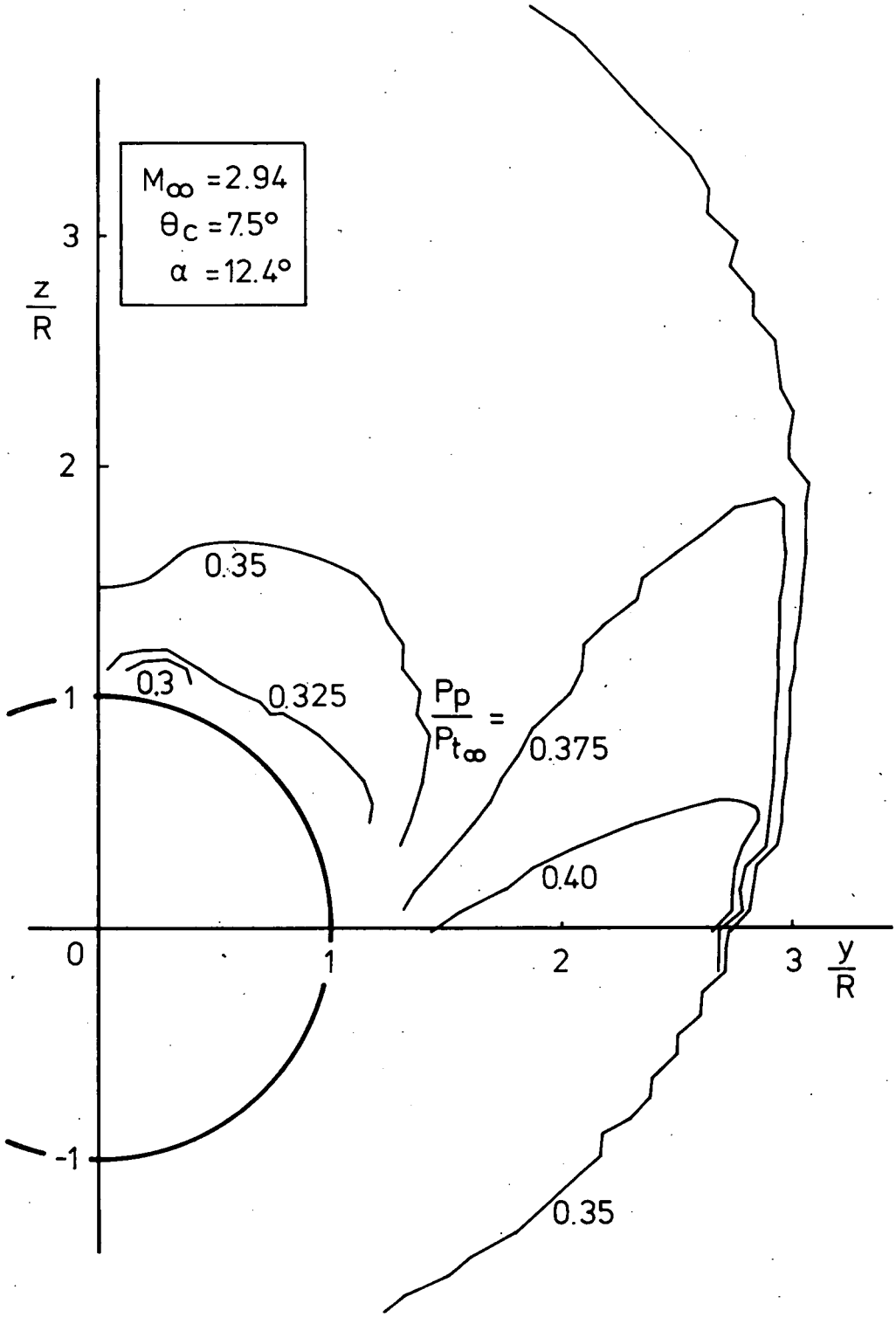

FIG.7: LINES OF CONSTANT PITOT PRESSURE.

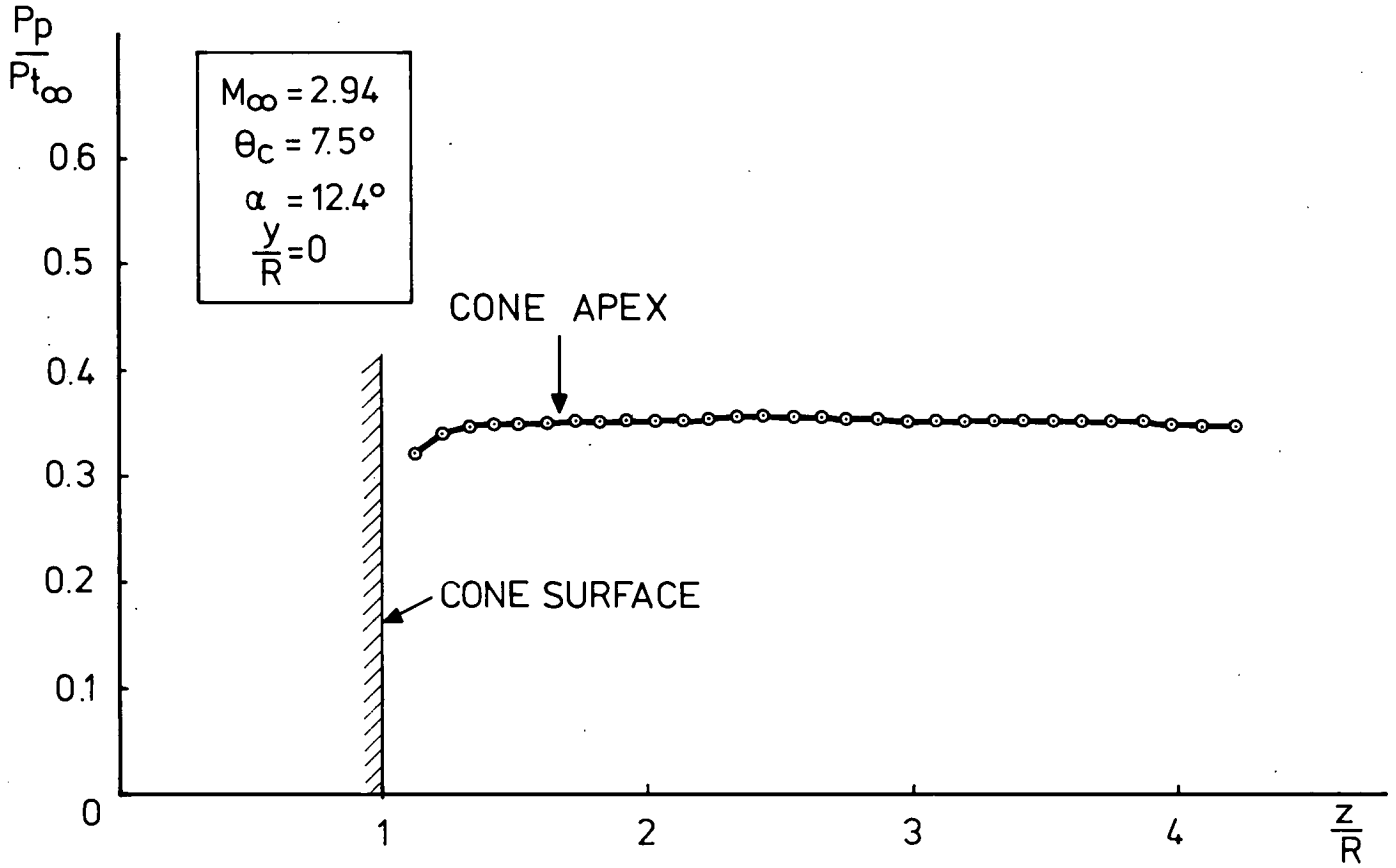

FIG.8 : PITOT PRESSURE IN THE LEEWARD PLANE OF SYMMETRY .

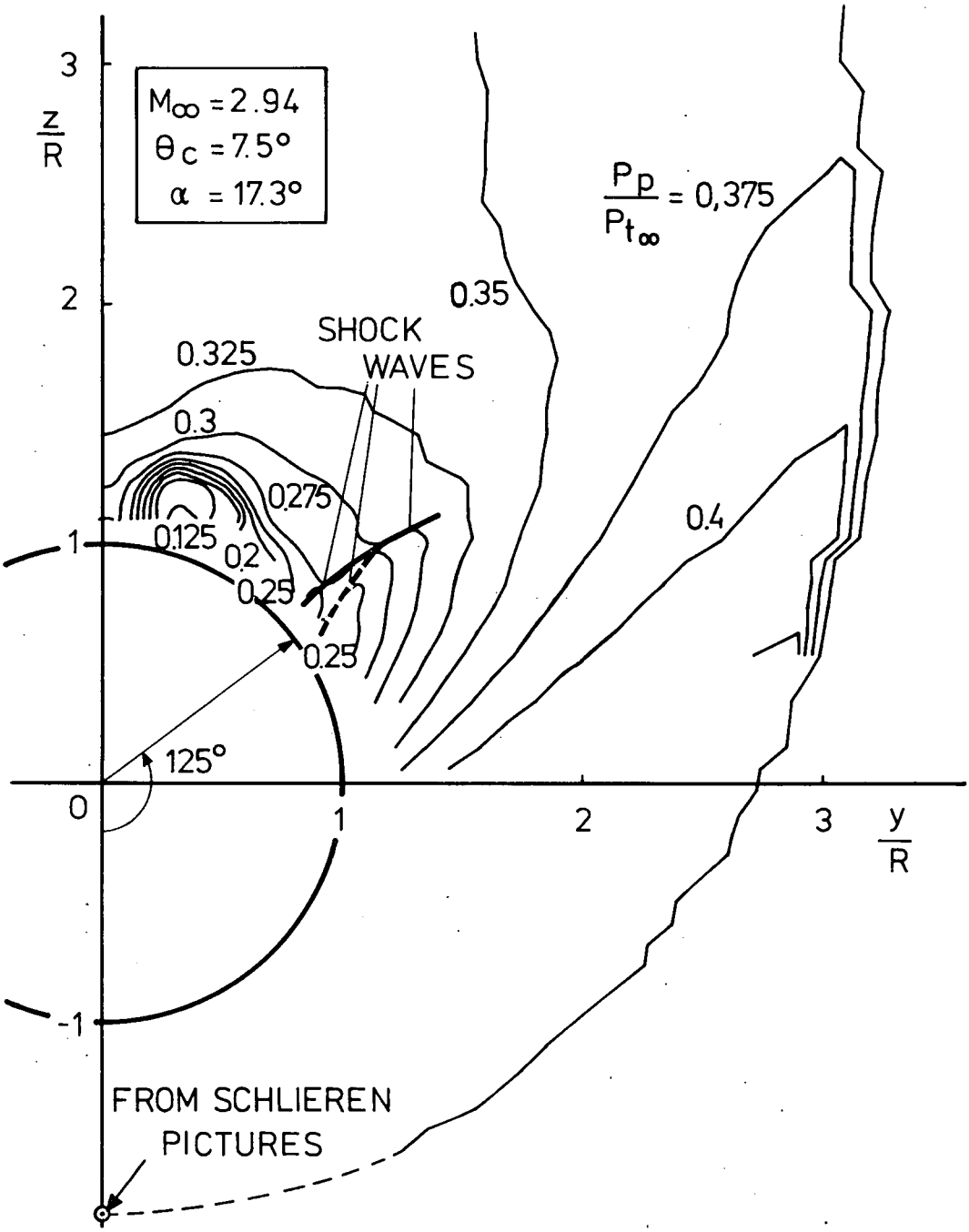

FIG.9:LINES OF CONSTANT PITOT PRESSURE.

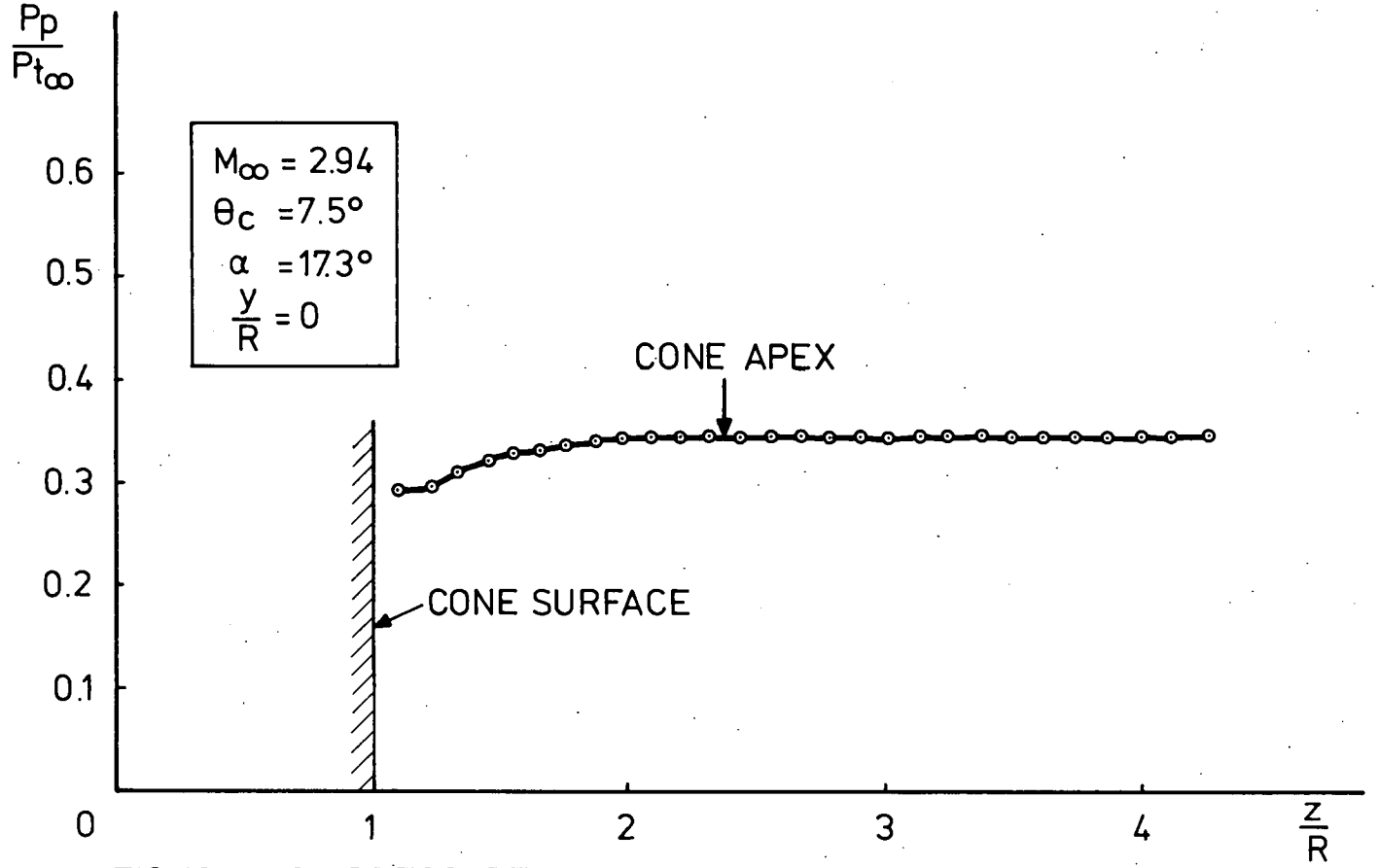

FIG.10: PITOT PRESSURE IN THE LEEWARD PLANE OF SYMMETRY.

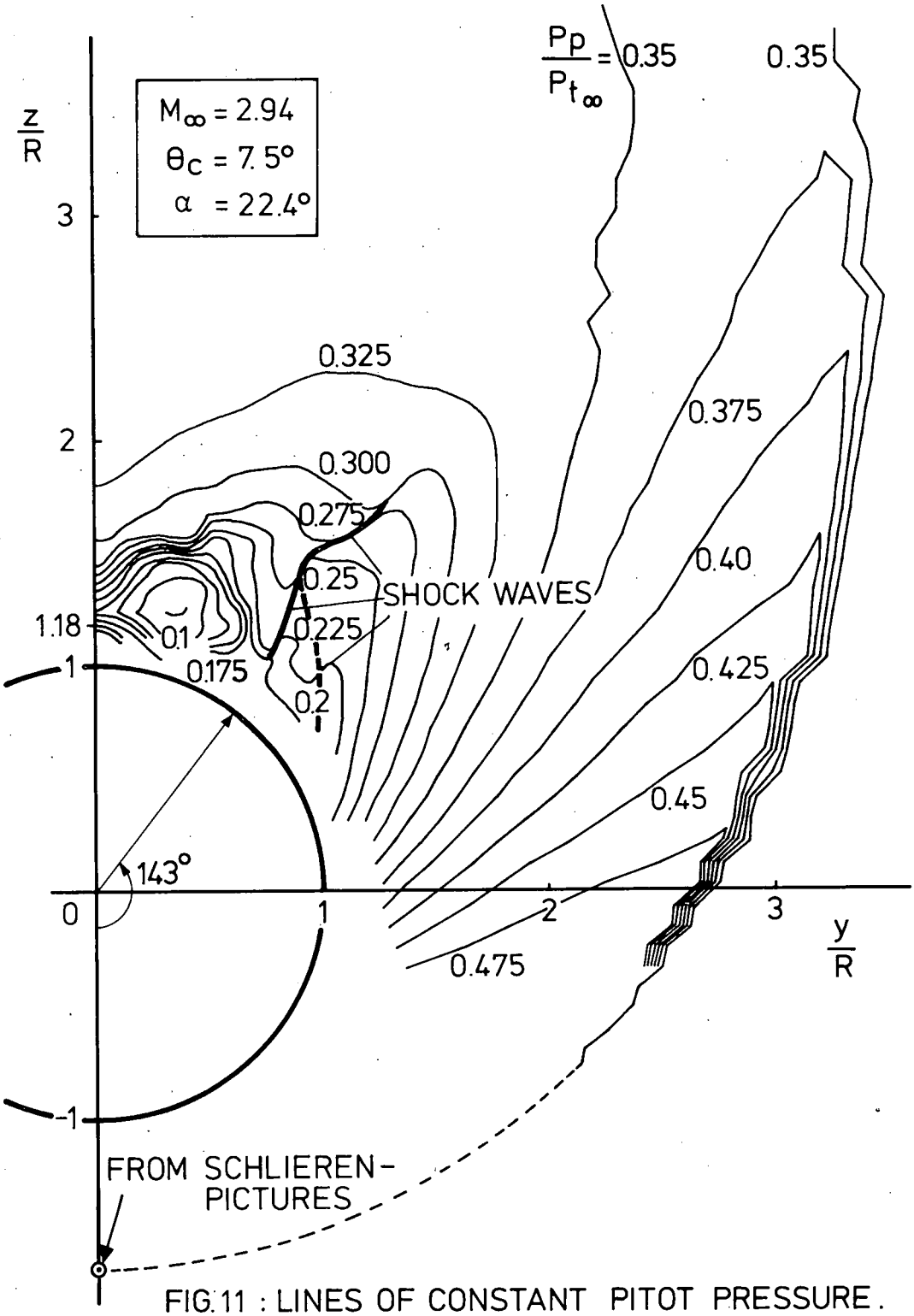

FIG.11 : LINES OF CONSTANT PITOT PRESSURE.

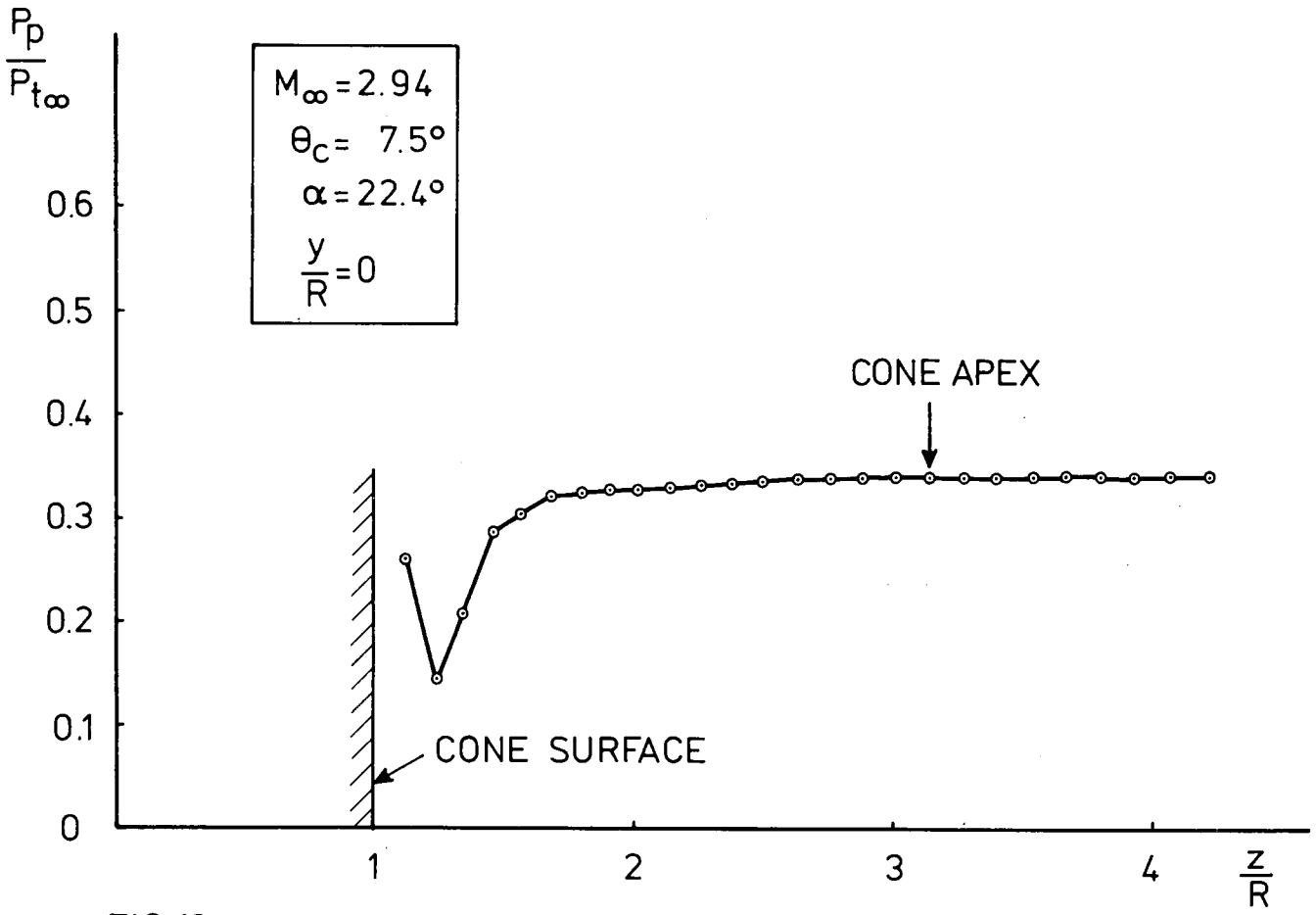

FIG.12 : PITOT PRESSURE IN THE LEEWARD PLANE OF SYMMETRY.

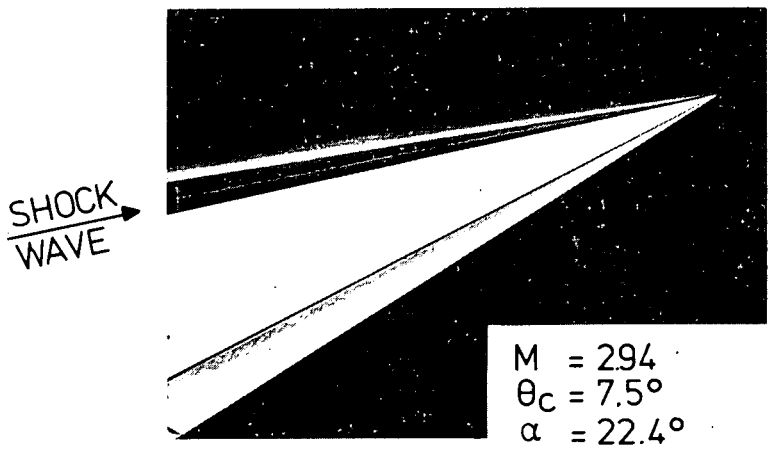

FIG. 13: SCHLIEREN PICTURE OF THE FLOW FIELD AT α = 22.4 DEG. M = 2.94 θ_c = 7.5 DEG.

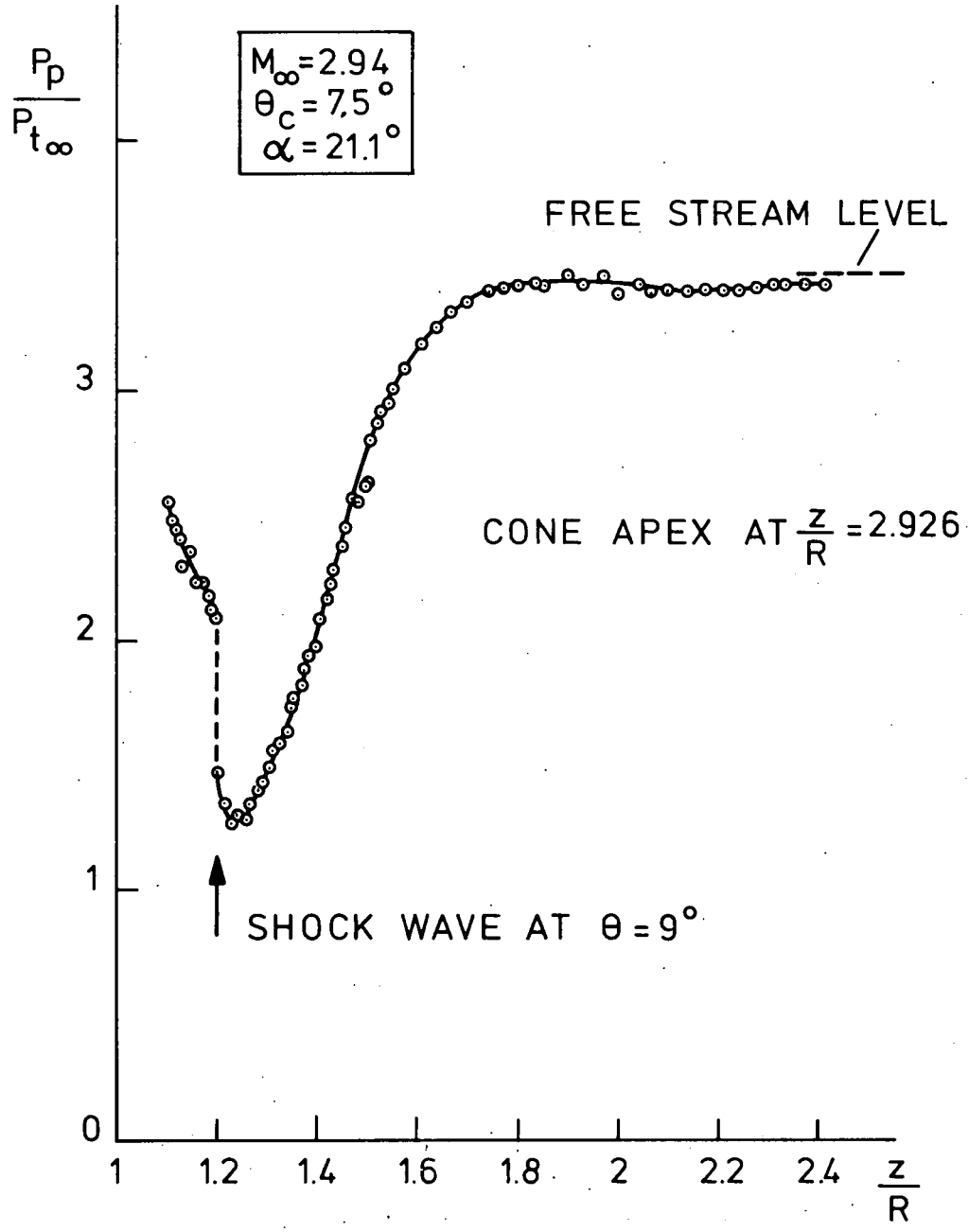

FIG .14 : PITOT PRESSURE TRAVERSE IN THE LEEWARD PLANE OF SYMMETRY.

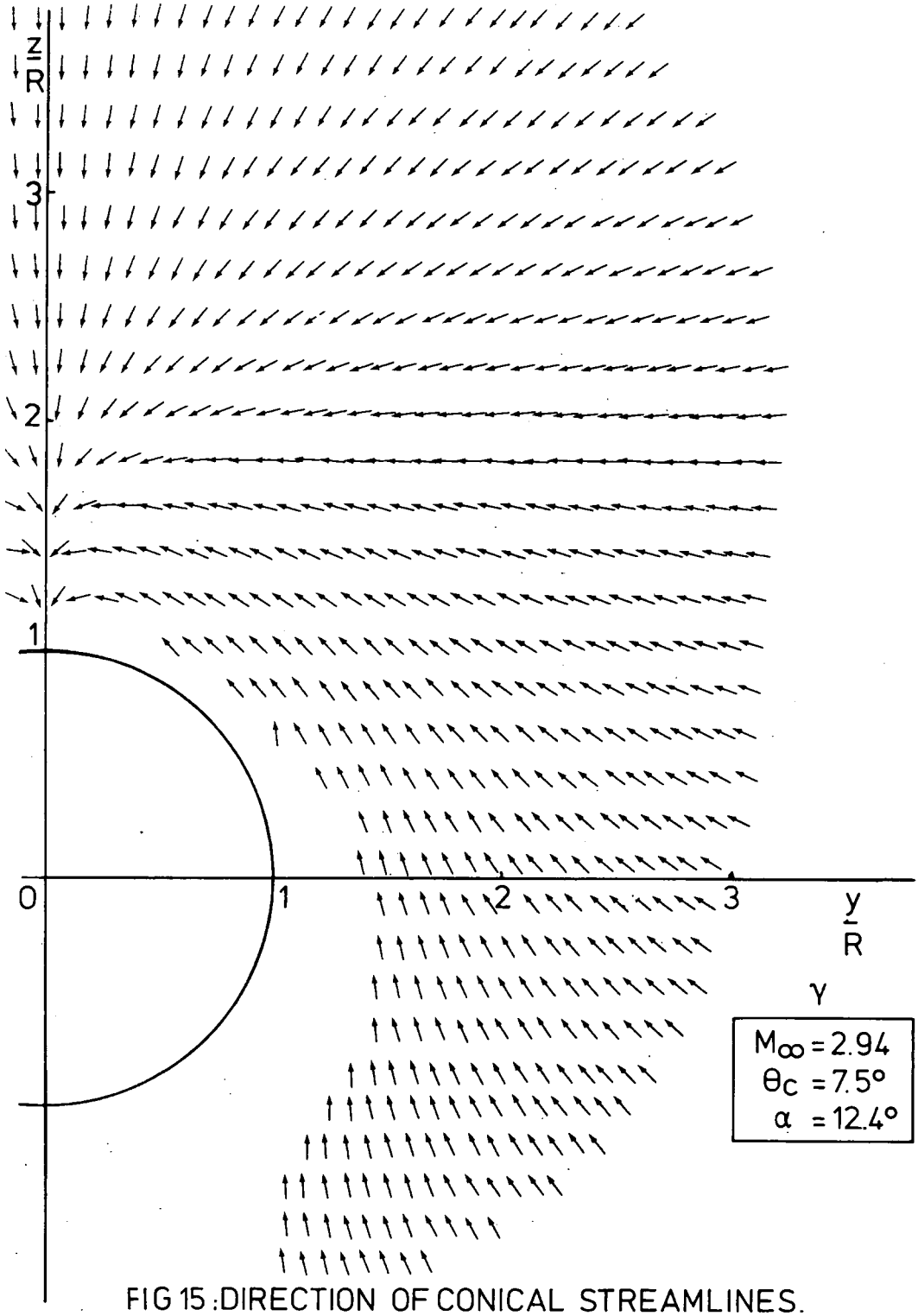

FIG 15 : DIRECTION OF CONICAL STREAMLINES.

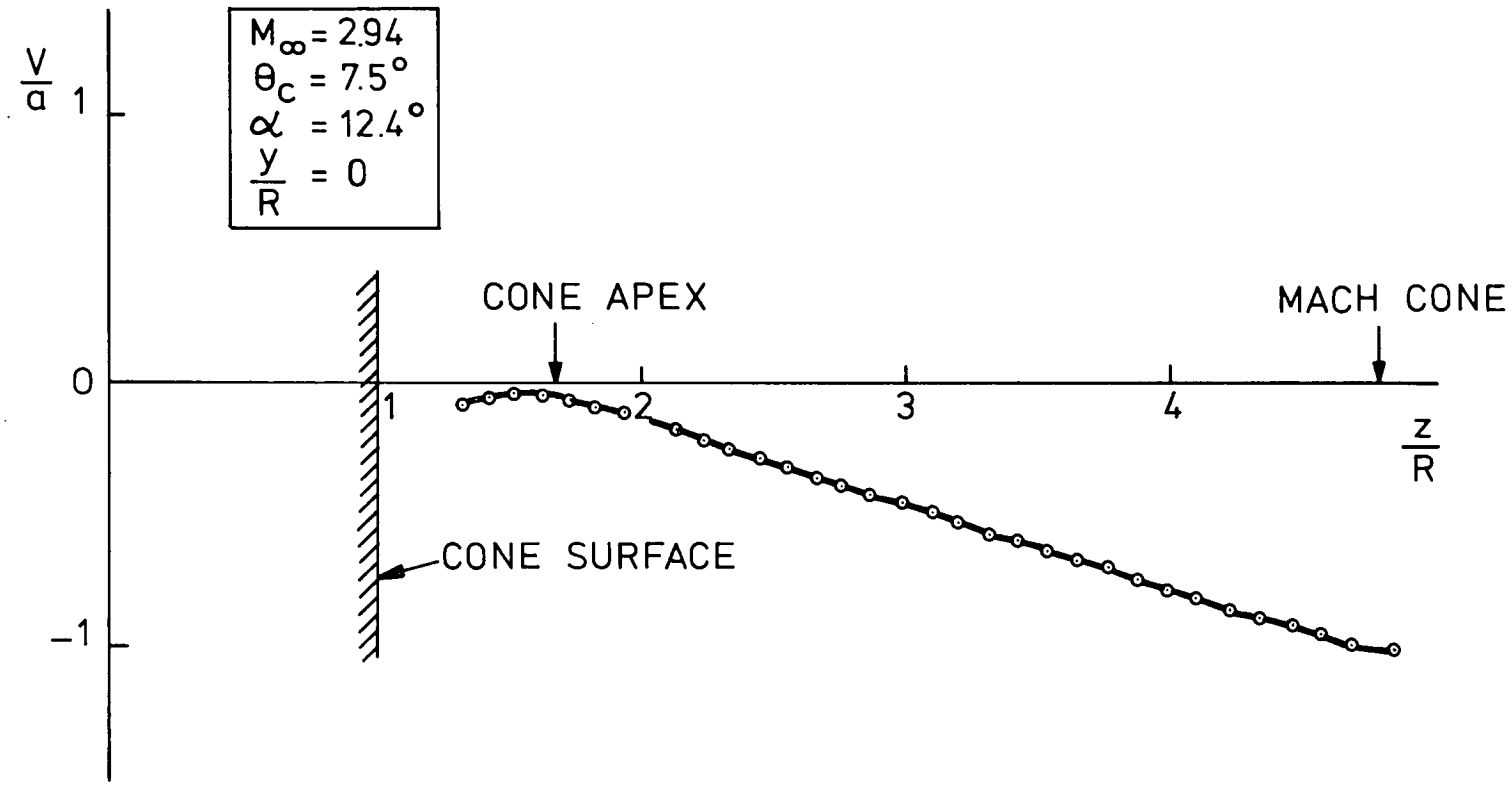

FIG .16: CONICAL MACH NUMBER IN THE LEEWARD PLANE OF SYMMETRY .

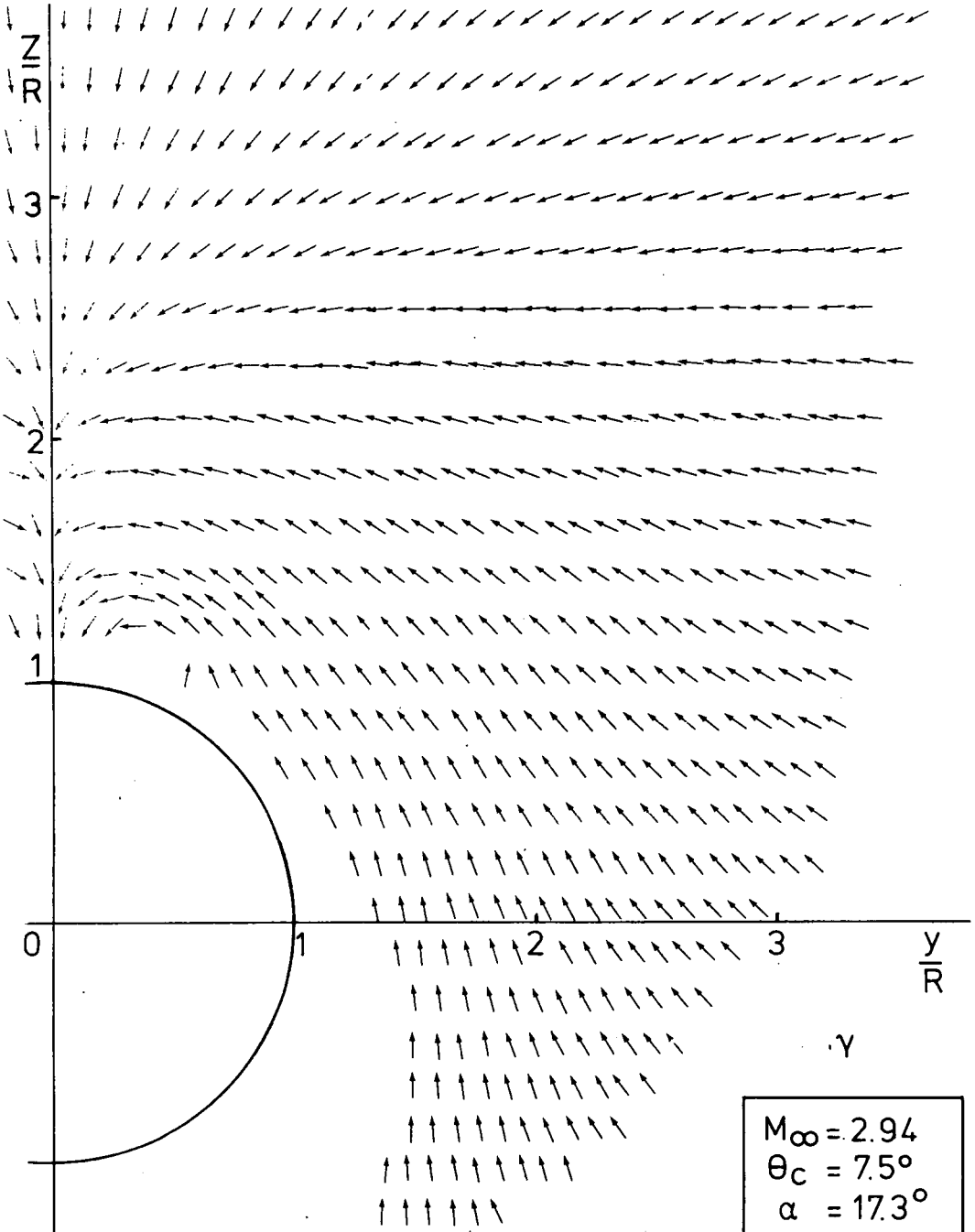

FIG.17: DIRECTION OF CONICAL STREAMLINES.

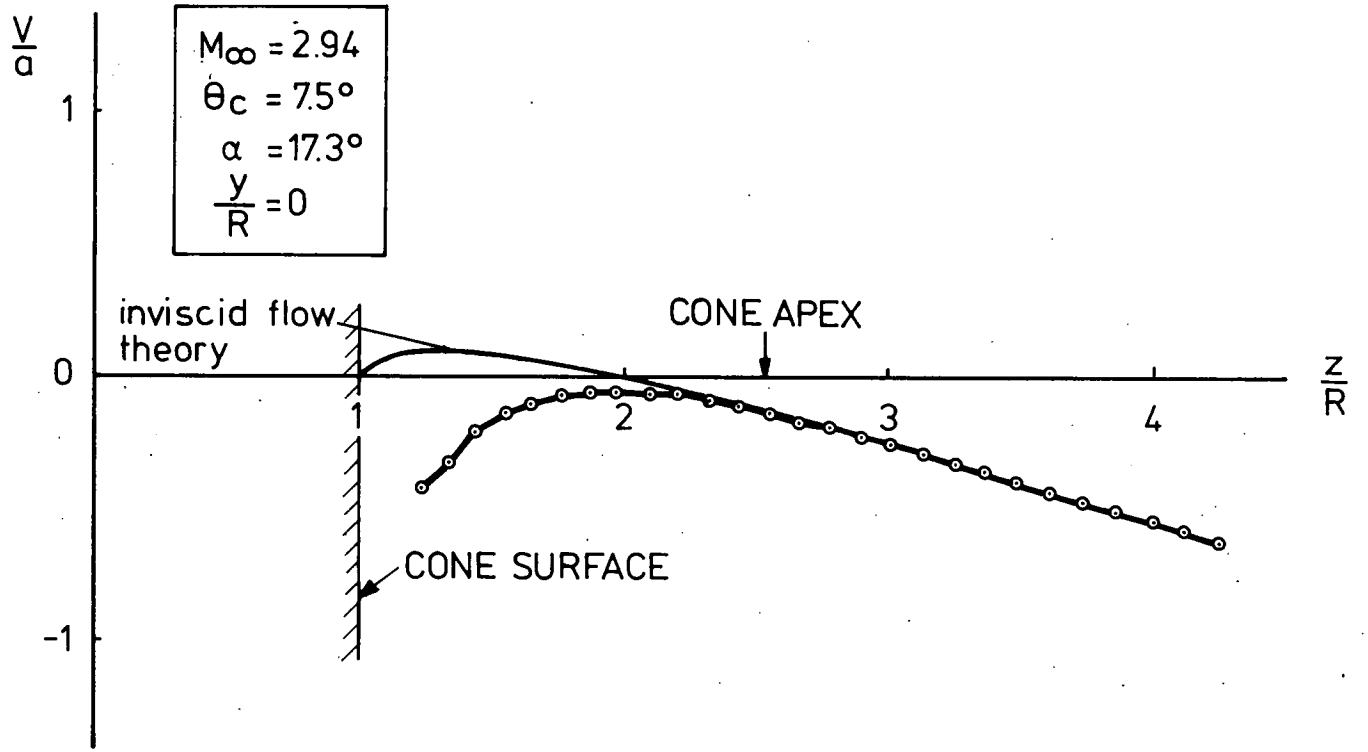

FIG. 18 : CONICAL MACH NUMBER IN THE LEEWARD PLANE OF SYMMETRY.

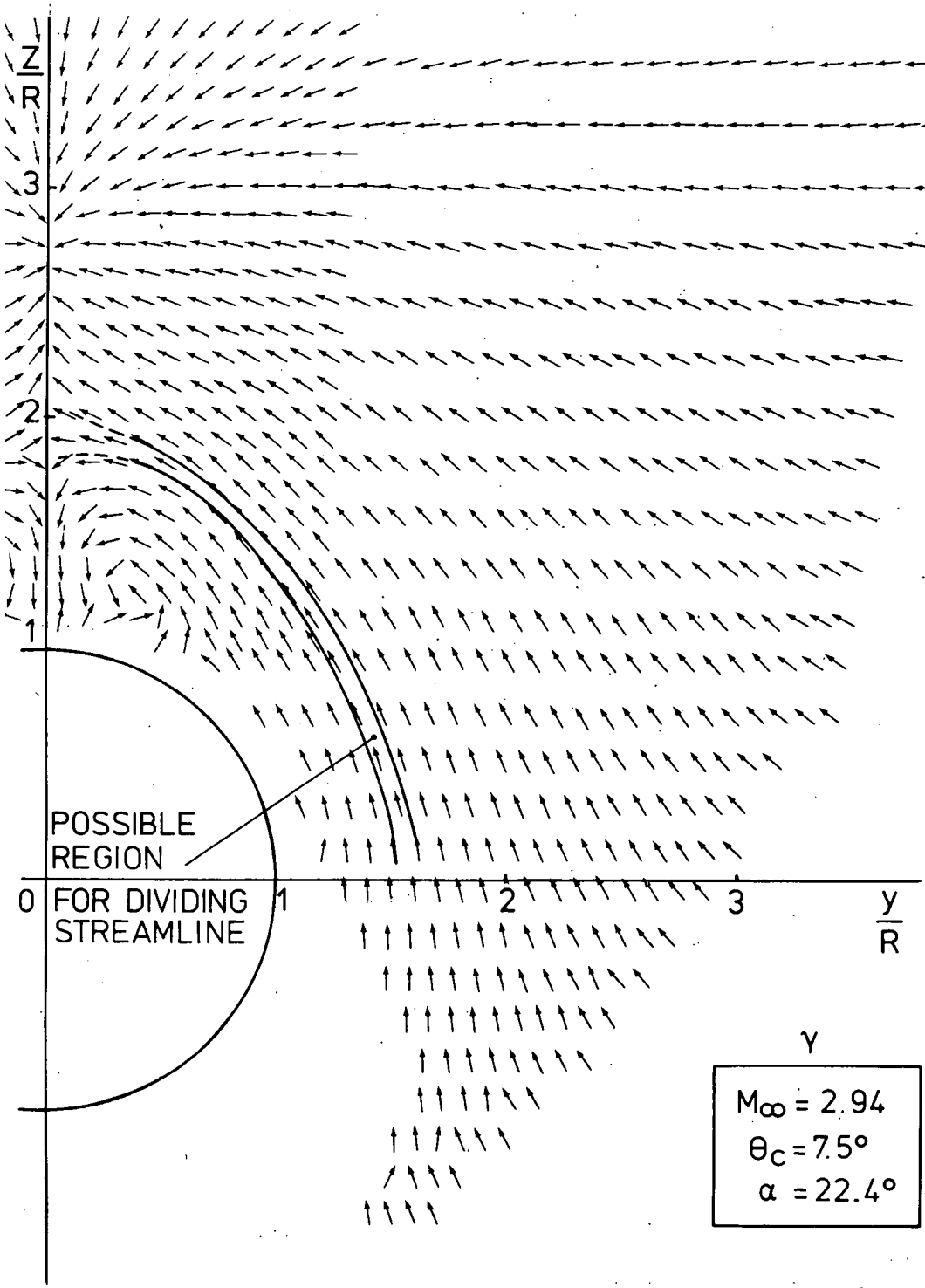

FIG.19: DIRECTION OF CONICAL STREAMLINES.

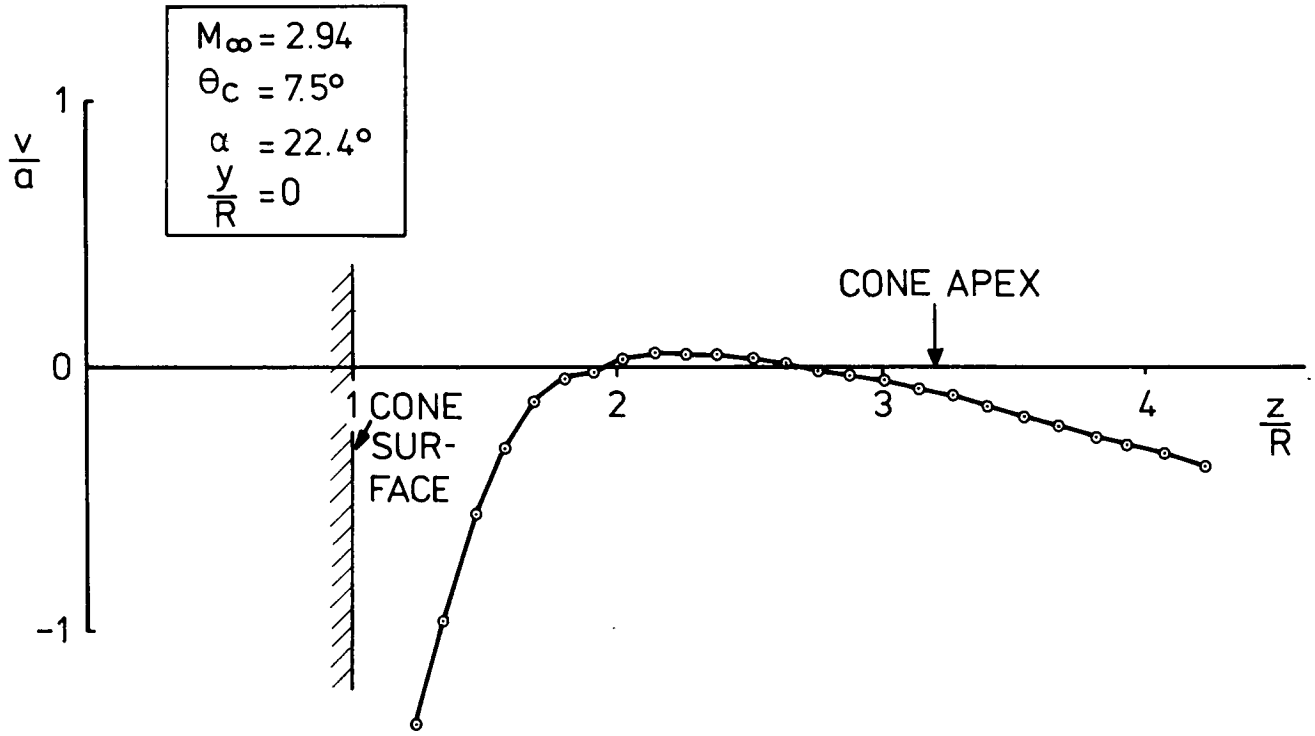

FIG.20: CONICAL MACH NUMBER IN THE PLANE OF SYMMETRY.

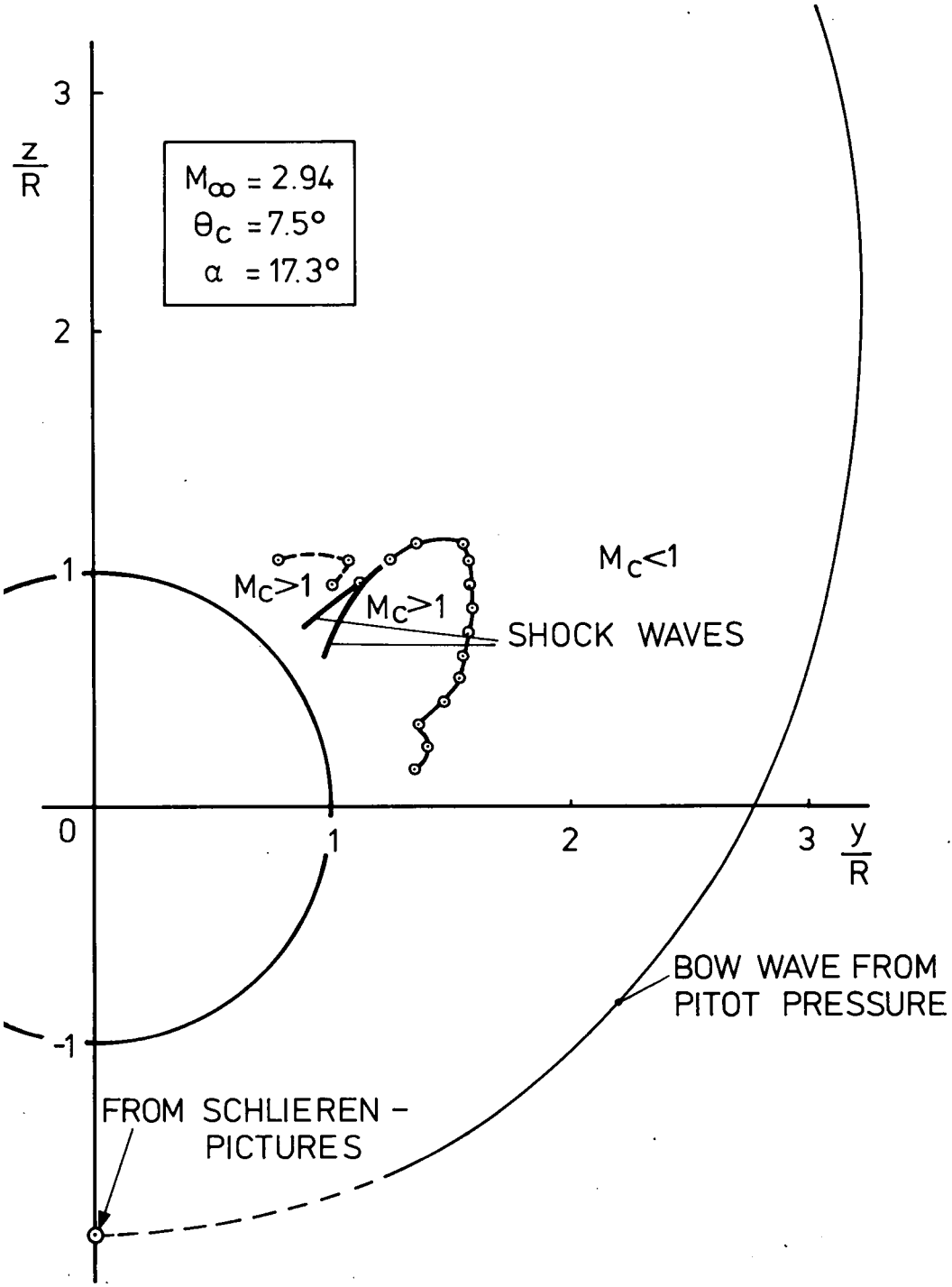

FIG.21: CONICAL MACH NUMBER REGIMES AND SHOCK WAVES.

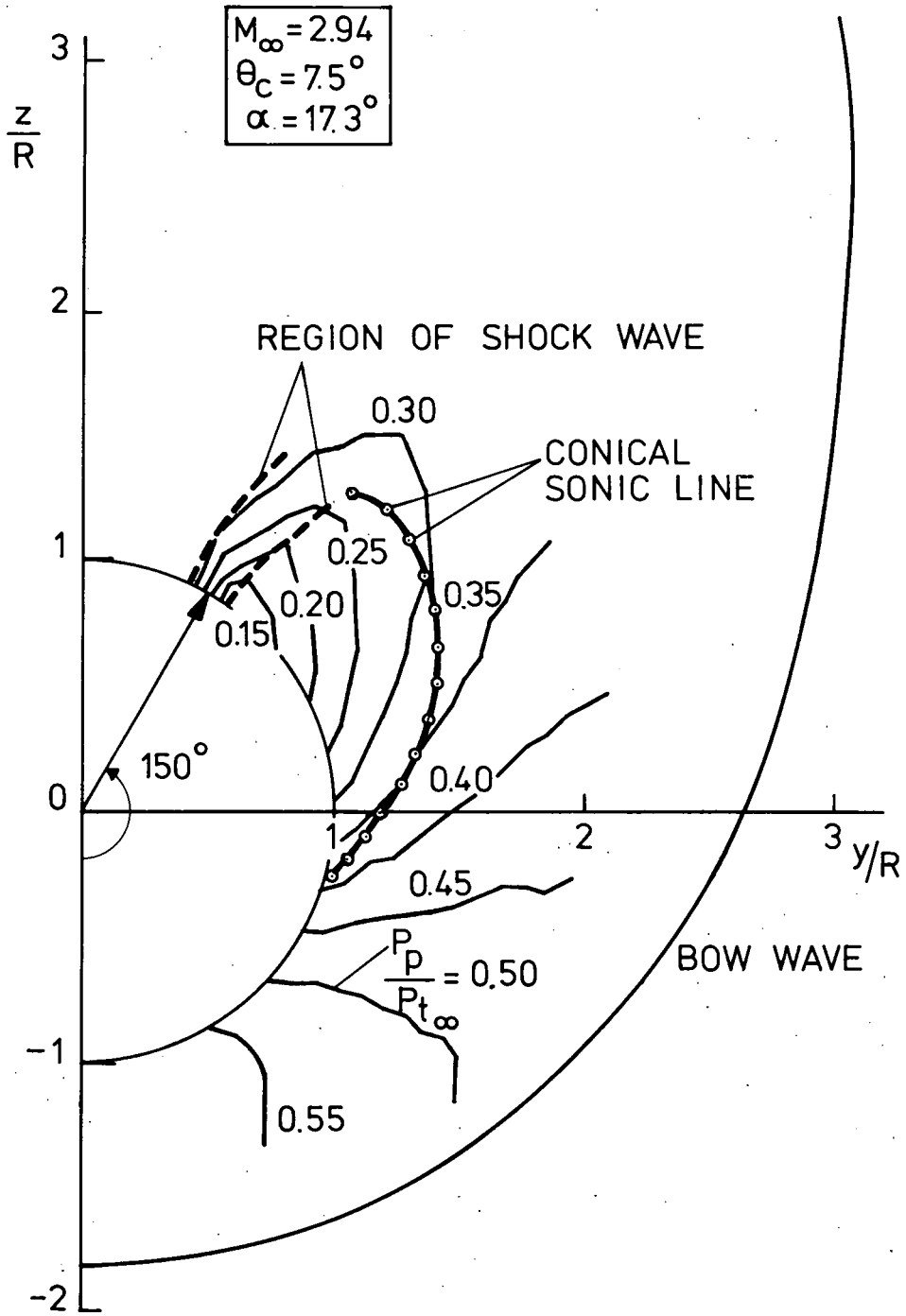

FIG.22: INVISCID FLOW FIELD CALCULATED USING A SHOCK CAPTURING TECHNIQUE

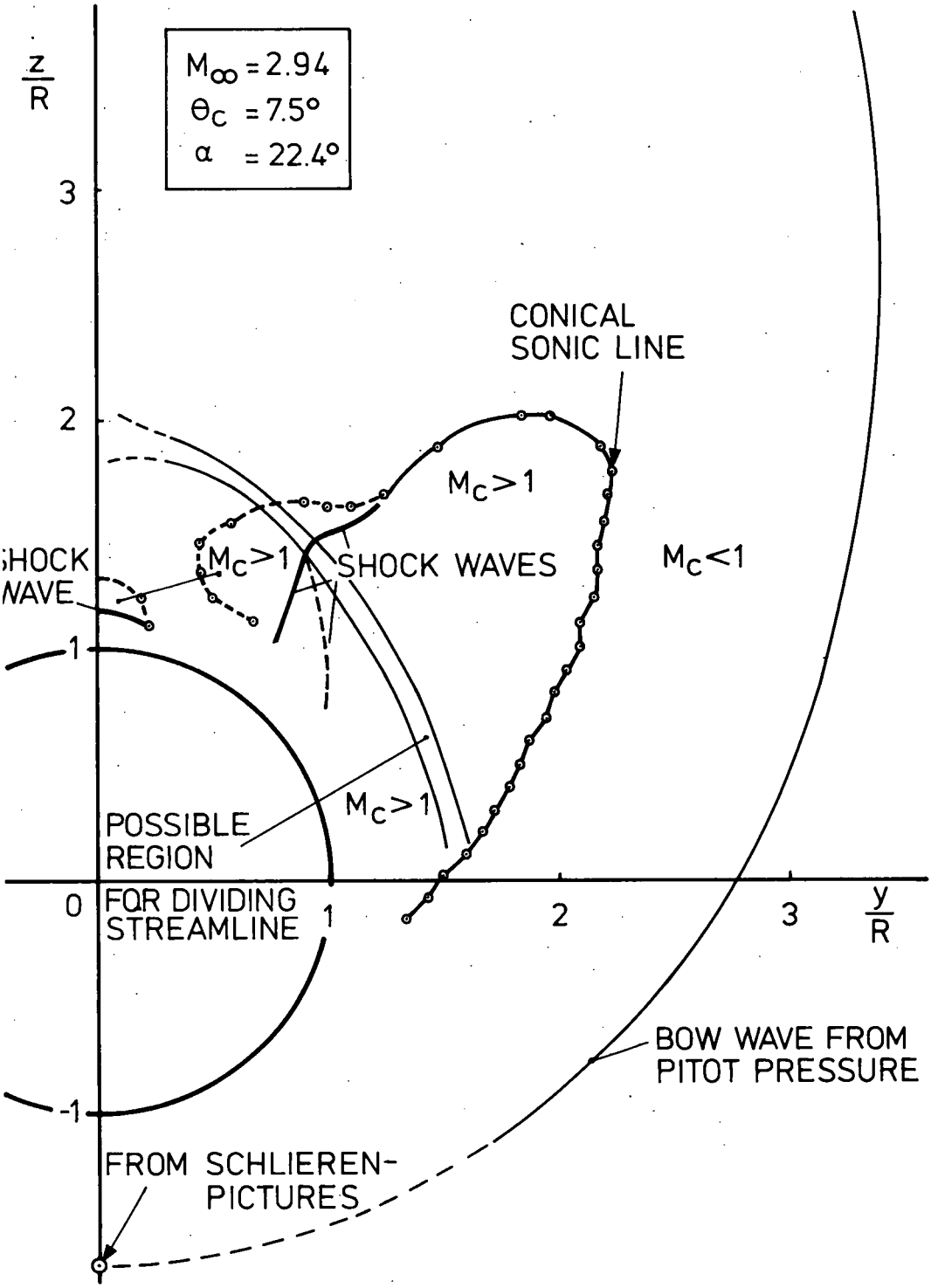

FIG.23: CONICAL MACHNUMBER REGIMES AND SHOCK WAVES.